



# Master Thesis

## Self-Shading and Ground-Shading of Agrivoltaic Systems Across Europe

submitted by

**Isabelle GRABNER, BSc**

in the framework of the Master programme

**Stoffliche und Energetische Nutzung Nachwachsender Rohstoffe  
(NAWARO)**

in partial fulfilment of the requirements for the academic degree

**Diplom-Ingenieurin**

Vienna, June 2025

Supervisor

Assoc. Prof. Priv.Doz.DI Dr.nat.techn. Johannes  
Schmidt  
Institute of Sustainable Economic Development  
Department of Economics and Social Sciences  
Universität für Bodenkultur Wien

Co-supervisor

Dr. Christian Mikovits MMSc.  
Institute of Sustainable Economic Development  
Department of Economics and Social Sciences  
Universität für Bodenkultur Wien



# Affidavit

I, Isabelle Grabner, hereby declare that I have authored this master thesis independently, and that I have not used any assistance other than that which is permitted. The work contained herein is my own except where explicitly stated otherwise. All ideas taken in wording or in basic content from unpublished sources or from published literature, as well as those which were generated using artificial intelligence tools, are duly identified and cited, and the precise references included.

I further declare that this master thesis has not been submitted, in whole or in part, in the same or a similar form, to any other educational institution as part of the requirements for an academic degree.

I hereby confirm that I am familiar with the standards of Scientific Integrity and with the guidelines of Good Scientific Practice, and that this work fully complies with these standards and guidelines.

Vienna, June 2025

---



# Acknowledgements

I would like to thank everyone, especially my supervisors Johannes Schmidt and Christian Mikovits, for the support I received during both the research and the writing process of this thesis. I am also deeply grateful to all the teachers who have provided me with guidance and accompanied me throughout my time at BOKU and the University of Vienna, as well as the fellow students I got to meet and collaborate with over the past years.

Special thanks go to my family, they have supported me through every important decision and made it possible for me to pursue my studies. Finally, I would like to thank my friends, who have been there for me during these years and managed to fill even difficult times with joy.



# Abstract

To mitigate climate change, replacing conventional energy sources with renewable energies is of highest importance. Photovoltaics is one of the most promising technologies in this context, but faces the problem of constrained land availability in Europe. Placing photovoltaic panels on agricultural land, also referred to as agrivoltaics, presents a solution to this. In addition to providing electricity, the use of agrivoltaics comes with additional benefits, such as providing shading to crops facing heat stress. Up to now, simulations of these shading effects are available for case study regions or on national scale, but not for larger regional extents, such as on the European level.

In this thesis, a computationally efficient model to calculate ground- and self-shading in agrivoltaic systems is developed and applied to five commonly used systems – tracking, backtracking, vertical, overhead and standard – to generate shading data for the whole of Europe. Ground-shading was found to be lowest in the overhead system, followed by the vertical setup. Similar amounts of shading were identified for the tracking and backtracking systems. The highest amount of shading was calculated for the standard system, which also generated particularly uneven shading when compared to other setups. Self-shading was overall the highest in the standard system for higher latitudes, but with amounts of shading at lower latitudes comparable to other systems.

The model used in this thesis can be combined with models simulating electricity generation and crop productivity to inform about the overall performance of agrivoltaic systems. Furthermore, other applications requiring shading information can also benefit from the simulation.



# Kurzfassung

Zur Eindämmung des Klimawandels ist es von großer Bedeutung, fossile Energieträger durch erneuerbare Alternativen zu ersetzen. Eine der wichtigsten Stromerzeugungstechnologien in diesem Kontext ist Photovoltaik, welche in Europa aber mit dem Problem von begrenzter Flächenverfügbarkeit konfrontiert ist. Eine gemeinsame Landnutzung durch Landwirtschaft und Solarpaneele, welche auch als Agri-Photovoltaik bezeichnet wird, stellt eine mögliche Lösung für dieses Problem dar. Neben der zur Verfügung gestellten Energie, könnte Agri-Photovoltaik auch andere positive Effekte haben, beispielsweise den Schutz von Nutzpflanzen vor Hitzestress durch zusätzliche Beschattung. Simulationen von Schatteneffekten sind bisher aber nur für einzelne Fallstudien oder für einzelne Länder durchgeführt worden, nicht aber für größere Regionen wie Europa.

In dieser Arbeit wird ein Modell zur Berechnung von Boden- und Selbstbeschattung in Agri-Photovoltaiksystemen entwickelt und auf einige, häufig genutzte Systeme angewandt, um die zuvor genannten Beschattungsparameter für Europa zu berechnen. Die simulierten Systemtypen umfassen nachgeführte Systeme mit und ohne Selbstbeschattungsvermeidung, vertikale und hoch aufgeständerte Anlagen sowie ein konventionelles System. Die niedrigste Bodenbeschattung konnte im hoch aufgeständerten System verzeichnet werden, gefolgt vom vertikalen System. Ähnliche Beschattungswerte wurden für die beiden nachgeführten Systeme berechnet. Die höchsten Werte wurden im konventionellen System erreicht, im Gegensatz zu den restlichen simulierten Systemen war die Bodenbeschattung in diesem auch besonders ungleichmäßig verteilt. Die insgesamt höchsten Selbstbeschattungswerte wurden ebenfalls im konventionellen System für höhere Breitengrade erreicht, wobei für niedrige Breitengrade mit anderen Systemen vergleichbare Resultate erreicht wurden.

Das in dieser Arbeit erstellte Modell kann in Zukunft mit Modellen, welche Strom- und landwirtschaftlichen Ertrag berechnen, kombiniert werden. Auch andere Anwendungen, welche detaillierte Schatteninformationen benötigen, können von der Simulation profitieren.



# Contents

<b>Affidavit</b>	i
<b>Acknowledgements</b>	iii
<b>Abstract</b>	v
<b>Kurzfassung</b>	vii
<b>List of Tables</b>	xi
<b>List of Figures</b>	xiii
<b>1. Introduction</b>	1
<b>2. Methods and Data</b>	3
2.1. Overview of Data Sources and Generated Data . . . . .	3
2.2. Simulated Agrivoltaic Systems . . . . .	4
2.2.1. Tracking System . . . . .	4
2.2.2. Backtracking System . . . . .	5
2.2.3. Vertical System . . . . .	5
2.2.4. Overhead System . . . . .	6
2.2.5. Standard System . . . . .	7
2.2.6. Overview of System Parameters . . . . .	7
2.3. Projection of Sun Beams onto E/W and N/S planes . . . . .	9
2.4. Repositioning for Tracking and Backtracking Systems . . . . .	10
2.4.1. Tracking System . . . . .	10
2.4.2. Backtracking System . . . . .	10
2.5. Shade Projected by Direct Sunlight . . . . .	11
2.5.1. Ground-Shading . . . . .	11
2.5.2. Self-Shading . . . . .	18
2.5.3. Percentage of Time Shaded . . . . .	28
<b>3. Results</b>	29
3.1. Average Shading . . . . .	29
3.1.1. Average Shading Depending on Latitude . . . . .	29
3.1.2. Average Shading Depending on Daytime . . . . .	31
3.1.3. Average Shading Over One Year . . . . .	34
3.2. Illuminated Time . . . . .	36

*Contents*

3.3. Distribution of Field Shading . . . . .	39
<b>4. Discussion</b>	<b>43</b>
<b>5. Summary</b>	<b>45</b>
<b>Bibliography</b>	<b>47</b>
<b>A. Appendix</b>	<b>51</b>
A.1. Panel Tilt in Standard System by Latitude . . . . .	51
A.2. Average Shading Depending on Daytime - Monthly Comparison . . . . .	52
A.3. Average Shading Depending on Daytime - Including/Excluding Horizons . . . . .	54
A.4. Average Shading Depending on Date - Including/Excluding Horizons . . . . .	56
A.5. Field Shading - Backtracking . . . . .	58

# List of Tables

2.1. System parameters . . . . .	8
A.1. Panel tilt by latitude for standard system . . . . .	51



# List of Figures

2.1.	This figure shows an overview of data sources and generated data. In this input data sets are shaded in green, final outputs are shaded in pink. Horizon data, as an intermediary output, is shaded in blue. White represents models and processes. . . . .	3
2.2.	Example of tracking system . . . . .	5
2.3.	Example of vertical system . . . . .	6
2.4.	Examples of overhead systems . . . . .	6
2.5.	Example of standard system . . . . .	7
2.6.	Projection of sun beams onto E/W and N/S planes . . . . .	9
2.7.	Ground-shading with split sunbeam components . . . . .	11
2.8.	Height difference of edges from base height . . . . .	12
2.9.	Coordinate system and position of PV panel for N/S aligned systems . . . . .	13
2.10.	Position of western shade corners . . . . .	14
2.11.	Position of eastern shade corners . . . . .	14
2.12.	Coordinate system and position of PV panel for E/W aligned systems . . . . .	15
2.13.	Position of northern shade corners . . . . .	16
2.14.	Position of southern shade corners . . . . .	16
2.15.	Field layout with vertical PV panels . . . . .	17
2.16.	Shade width in tracking system . . . . .	19
2.17.	Offset calculation . . . . .	19
2.18.	Offset and shade length in tracking system . . . . .	20
2.19.	Shade width in vertical system . . . . .	21
2.20.	Sun angles in N/S plane for standard system . . . . .	22
2.21.	Shade width in standard system . . . . .	23
2.22.	Offset and shade length in standard system . . . . .	24
2.23.	Sun angles in E/W plane for overhead system . . . . .	25
2.24.	Shade width in overhead system . . . . .	26
2.25.	Offset and shade length in overhead system . . . . .	27
2.26.	Grid layout for percentage of time shaded calculations . . . . .	28
3.1.	Shading over latitudes - including nighttime . . . . .	29
3.2.	Shading over latitudes - daytime . . . . .	30
3.3.	Comparison of calculated ground-shading with different time intervals . . . . .	31
3.4.	Shading by daytime . . . . .	32
3.5.	Shading by daytime at different times of the year in vertical system . . . . .	33
3.6.	Shading in vertical system by daytime with and without horizons . . . . .	33

## *List of Figures*

3.7. Shading in vertical system by daytime with and without horizons for Ennstal region . . . . .	34
3.8. Shading over one year . . . . .	35
3.9. Shading in vertical system by date with and without horizons . . . . .	36
3.10. Illuminated time across Europe . . . . .	37
3.11. Global horizontal irradiance under clear sky conditions on the 1 <sup>st</sup> of July at different latitudes . . . . .	38
3.12. Distribution of illuminated time across Europe . . . . .	38
3.13. Field shading in different systems . . . . .	39
3.14. Field shading in tracking system with altered parameters . . . . .	40
3.15. Field shading changes by latitude . . . . .	41
A.1. Shading by daytime at different times of the year in tracking system . . .	52
A.2. Shading by daytime at different times of the year in backtracking system .	52
A.3. Shading by daytime at different times of the year in overhead system . .	53
A.4. Shading by daytime at different times of the year in standard system . .	53
A.5. Shading in tracking system by daytime with and without horizons . . . .	54
A.6. Shading in backtracking system by daytime with and without horizons .	54
A.7. Shading in overhead system by daytime with and without horizons . . . .	55
A.8. Shading in standard system by daytime with and without horizons . . . .	55
A.9. Shading in tracking system by date with and without horizons . . . . .	56
A.10. Shading in backtracking by date with and without horizons . . . . .	56
A.11. Shading in overhead by date with and without horizons . . . . .	57
A.12. Shading in standard system by date with and without horizons . . . . .	57
A.13. Field shading in backtracking system . . . . .	58
A.14. Field shading change by latitude in backtracking system . . . . .	58

# 1. Introduction

Climate change is an important issue, which today's world is facing. It is the cause for an increase in the frequency of droughts and heat waves as well as rising global temperatures among a plethora of other issues [1, 2, 3, 4]. In the face of this challenge, there is a need to replace non-renewable energy sources with renewable alternatives to reduce carbon emissions. One such source is solar energy. However, due to competing land needs from the agricultural sector, there is a lack of available area to be used exclusively for solar energy generation in Europe [5, 6].

The consequences of climate change listed above also present a challenge for modern agriculture. There is a need to mitigate the effects on crop production as well as livestock to ensure food security [7, 8].

In agrivoltaic systems agricultural and solar energy generation are combined by installing photovoltaic panels alongside crops. This approach could simultaneously address the lack of land available for photovoltaic systems, as well as mitigate the issues faced by agriculture due to climate change by providing shading to crops. Additionally, a successful implementation could lead to higher overall productivity per unit of area [9], while at the same time having the potential to make a positive impact on biodiversity [10, 11].

There are currently only a very limited number of agrivoltaic systems installed, these are mostly located in China, the USA and Europe [12]. In Germany, for example, there are eleven experimental sites listed by the Fraunhofer Institute as of 2024 [13]. Challenges for the adoption of agrivoltaic systems are manyfold and include policy related topics, such as a lack of financial support and a long approval process, a lack of data on effects on crop growth, limited awareness among farmers as well as a rejection due to the visual impact on landscapes [14]. There are however some early successes to be noted, besides additional energy generation. On one site, photovoltaic panels were installed above apple trees, protecting the crops from heavy rain, hail and storms. Additionally, a decreased need for fungicides due to lower humidity could be noted [15]. Agrivoltaic systems have also been experimentally shown to only slightly decrease and in some cases even increase yields depending on the shade tolerance of crops and climatic conditions. For instance, increases in production were noted for potato and winter wheat in the hot and dry summer of 2018 [16], implying a potential for increased benefits in the future due to climate change induced temperature increases.

There are several aspects of agrivoltaic systems, which are the subject of current studies. These include effects on temperature [16, 17], rain distribution [16, 18], crop growth [16, 19, 20, 21], energy output [22] and effects on land-use intensity [10]. Shading directly affects crops, in the case of ground-shading and energy output, in the case of self-shading.

In the context of this thesis ground-shading refers to the shade projected on the ground

## *1. Introduction*

by the photovoltaic panels. Self-shading describes shade cast by panels onto other panels in a given setup. Both aspects are defined as the shade resulting from direct solar irradiation, while diffuse lighting is not taken into account. Photovoltaic setups in all locations are treated as being located on even ground for the purposes of this study.

Results specifically regarding shading in different agrivoltaic systems can be found in several studies. For example, in a comparative analysis on agrivoltaic systems, Niazi and Victoria show changes in field irradiation for a static tilt, a single-axis tracking and a vertical system for a specific location in Europe [23]. Similarly, irradiation changes calculated for a static system and at a latitude of  $42^\circ$  can be found in [9]. Other studies model irradiance data under agrivoltaic systems on a small scale using ray tracing [24]. However, there is presently a lack of analysis regarding shading caused by agrivoltaic systems for large areas. The main goal of this thesis is to create a model which can be used to simulate self- and ground-shading for arbitrary photovoltaic systems, and which is computationally sufficiently efficient to calculate shading for large areas. While this model may be used for alternate applications in the future, in this thesis it will be applied to standard examples of agrivoltaic systems, for which shading will be simulated across all of Europe for a whole year. The resulting data is going to be analysed with respect to the temporal as well as the geographical component. The primary research subject is an analysis of the differences in ground- and self-shading across several common types of agrivoltaic systems.

Another aspect treated in this thesis is the influence of the geography surrounding a location, which is incorporated in the form of horizon elevation. For this, there will be an examination of the change in irradiated time over the course of one year across Europe. Additionally, the influence of the inclusion of horizon data on ground- and self-shading data will be analysed briefly.

## 2. Methods and Data

### 2.1. Overview of Data Sources and Generated Data

An overview of the used data sources and the main results generated in the scope of this thesis can be seen in Figure 2.1.

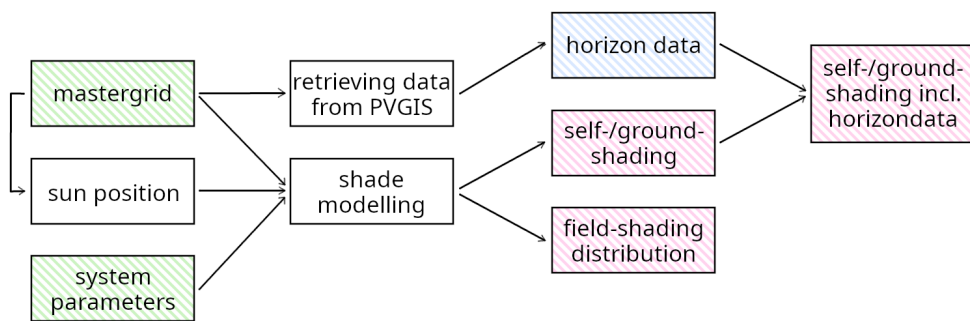


Figure 2.1.: This figure shows an overview of data sources and generated data. In this input data sets are shaded in green, final outputs are shaded in pink. Horizon data, as an intermediary output, is shaded in blue. White represents models and processes.

One of the main inputs used in the analysis is a GIS mastergrid, which is frequently used for the simulation of crop outputs at several institutions (e.g. BOKU University, International Institute of Applied Systems Analysis). It is a 1km by 1km grid representing Europe and contains approximately 5 million cells. For the modelling of shading in agrivoltaic systems, the main input used from the mastergrid, is the extent of latitudes for which the agrivoltaic systems are modelled. Additionally, the mastergrid was used to generate a dataset containing horizon data for all grid cells. This dataset contains the horizon elevation around a location with a resolution of  $7.5^\circ$ . The data was sourced from PVGIS [25].

Another data source used is summarized as system parameters, it contains all chosen measurements regarding the simulated agrivoltaic systems. The used parameters as well as their sources are described in detail in Section 2.2.

Lastly, a model was used to calculate the position of the sun depending on location, date and time, namely the solarposition function of the python module pvlib [26].

The data sources described above were used to model shading in several agrivoltaic

## 2. Methods and Data

systems for a whole year. This was done for latitudes contained in the mastergrid at  $1^{\circ}$  steps and along a set longitude. The program used for has been tested for all included system types, relevant scripts and tests can be found at [https://github.com/isagrabner/agri-pv\\_ground\\_and\\_self\\_shading](https://github.com/isagrabner/agri-pv_ground_and_self_shading) [27]. The resulting outputs include self- and ground-shading values at 15 minute time steps as well as the distribution of field shading for each system type.

In a separate step, horizon data was merged with the generated shading data. For this process, the azimuth of the sun at a given date, time and location was approximated with the closest azimuth available in the horizon data, which has a resolution of  $7.5^{\circ}$ . This data was included in the dataset containing self- and ground-shading. During the merger the elevation of the sun was compared to the elevation of the horizon at that azimuth, to determine whether direct sunlight is present at that time and location.

A similar process was conducted to calculate the total illuminated time on different days throughout the year for all mastergrid cells.

In the following sections an overview of the modelled agrivoltaic systems will be given before describing processes used in the handling of sun positions and tracking systems. Lastly, a detailed description of how ground- and self-shading was calculated within the generated model will be given.

## 2.2. Simulated Agrivoltaic Systems

Several common types of photovoltaic systems, which have been simulated in this thesis, will be described in this section. Systems included here are tracking systems, vertically mounted panels, elevated systems, also called overhead systems here and lastly fixed standard panels, see also [28]. An overview of the specific parameters chosen for each of these systems in this thesis will be given in 2.2.6.

### 2.2.1. Tracking System

There are several common types, which are split into single- and dual-axis tracking systems [13]. Dual-axis tracking systems are able to be adjusted freely, according to the position of the sun. In single-axis tracking systems panels are fixed along one axis and can be adjusted along the other. Both variants are generally used to optimize energy generation, but panel positions can also be adjusted with the goals of protecting against hail or extreme radiation [28], for cleaning purposes and for better access to crops, when necessary. Tracking systems are generally used over non-permanent crops, like maize [29], but can also be used in combination with permanent crops, like fruit trees [30]. For the latter, systems are installed at an elevated position, similar to the overhead systems described later.

Figure 2.2 shows an example of a single-axis tracking system. In this system, panel rows are usually parallel to the north/south direction. A system like this, with north/south aligned panel rows, is used for simulation in this thesis. A description of the method used for panel tilt adjustment can be found in 2.4.1. The parameters used for the modelled

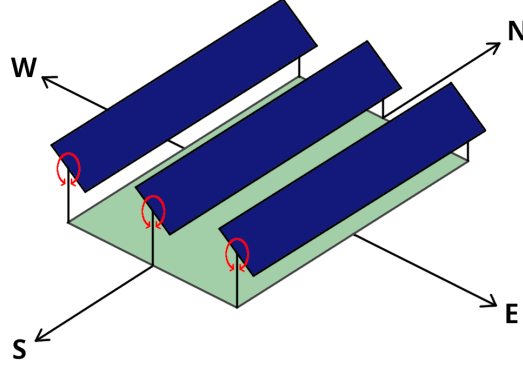


Figure 2.2.: Example of tracking system

tracking system were taken from [31]. The module type used is Canadian Solar's CS3W-420P HiKu, it is listed for non-bifacial modules in the cited paper. Specifications were obtained from [32].

### 2.2.2. Backtracking System

Backtracking systems are largely similar to the tracking systems described above. The notable difference in this setup is the altered panel adjustment. In this system panel tilt is set such that shading on neighbouring panel rows is avoided. This change primarily affects panel positioning at times close to sunrise and sunset, where high self-shading occurs. The purpose of said adjustments is to improve energy generation at these times [33]. The type of panel used for simulations is the same as the one described in the section about tracking systems.

### 2.2.3. Vertical System

In this system, panels are mounted vertically. They can be aligned freely depending on terrain conditions. Panels may be placed in parallel to east/west direction, but are most commonly aligned along the north/south direction. The former orientation is an improvement with regard to energy output, the latter is more effective for crop production [24]. Bifacial panels are commonly used in these setups [28]. A benefit of using vertical systems is the lack of interference with rainwater distribution [28, 18]. Vertical systems are commonly used alongside non-permanent crops, examples include maize, rapeseed, soybean [34], oats and potatoes [1].

A vertical system aligned along the north/south direction is shown in Figure 2.3. In this thesis a system like this is used for simulations. Measurements for this type were taken from [34], a matching bifacial module by JA Solar (JAM 54D40-450/LB) was used as a reference.

## 2. Methods and Data

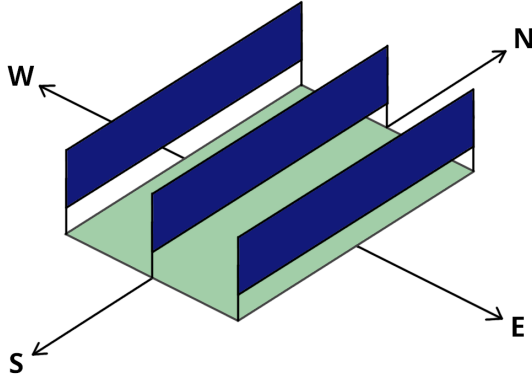


Figure 2.3.: Example of vertical system

### 2.2.4. Overhead System

In this thesis, the term overhead system is used to collectively refer to photovoltaic systems installed at a fixed angle and with a large clearance. The purpose of the high elevation in these systems is unimpeded management of crops and to accommodate the height of crops grown beneath them. The panel rows in these systems can be aligned along the north/south or east/west direction. Panels can all have the same tilt [35] or be arranged in a roof-like orientation [36], examples can be seen in Figure 2.4. In addition to energy generation, overhead systems may protect crops from extreme weather events like hail and sunburn. As such they can act as an alternative to traditional methods of protection like hail nets [35]. They are generally used for permanent crops, like fruit trees or in vineyards.

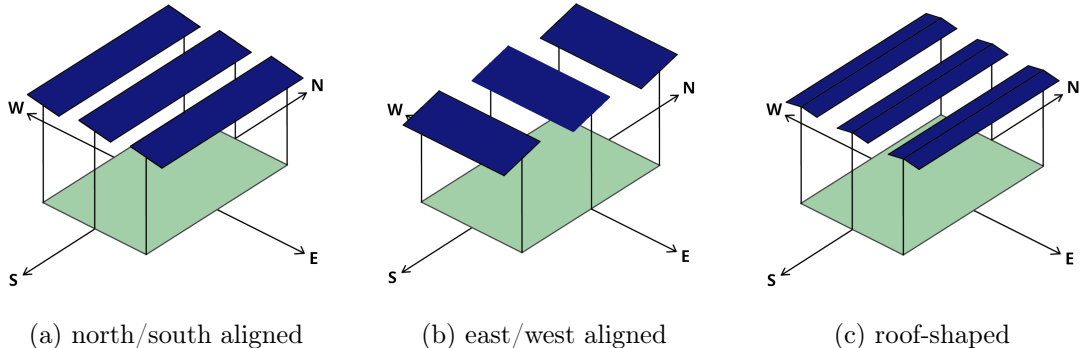


Figure 2.4.: Examples of overhead systems

In this thesis, the type of overhead system modelled is north/south aligned, as shown in Figure 2.4a. This system's measurements were taken from [36]. The description of the panel types used in the implementation of an overhead system described in this news

## 2.2. Simulated Agrivoltaic Systems

article matches the module plentiSOLAR Excellent Glass/Glass 170 M35, a description of which can be found at [37]. The slight panel tilt chosen for simulations is meant to facilitate self-cleaning during rain events.

### 2.2.5. Standard System

The setup in this system is similar to photovoltaic installations, which do explicitly facilitate agricultural use. The panel rows are aligned parallel to the east/west direction, they face south and have a fixed tilt. In Europe, tilt angles range between roughly  $30^\circ - 40^\circ$  [38]. If there is sufficient spacing, crops may be planted between panel rows [13]. This space may also be used in animal husbandry as a grazing area [39].

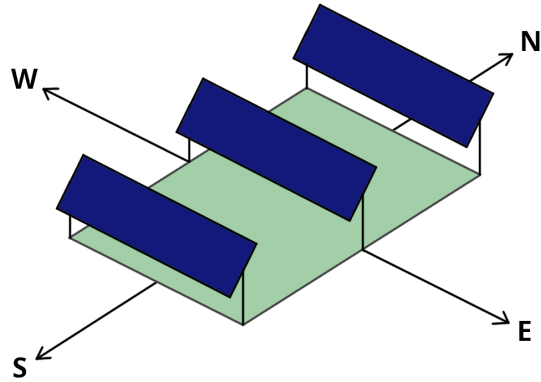


Figure 2.5.: Example of standard system

Figure 2.5 shows an example of this setup.

The panel distance used in modelling this system is set such that the gap between panels is close to the panel length as seen from a bird's-eye view. Since the optimal panel tilt in this system is latitude dependent, the theoretical panel distances and number of panel rows vary. The parameters chosen for simulations match with the southernmost simulated latitudes, which have the smallest tilt angles (and for this reason also have the largest distances between panels and smallest number of possible rows). Based on the chosen spacing, namely a 50/50 area split from bird's-eye view, 12 and 13 rows would be possible at higher latitudes. This would however also introduce increased self-shading. Because of this and in the interest of consistency, the panel distance and number of rows given in table 2.1 were used for all latitudes.

A non-bifacial PV model by Canadian Solar (CS3W-420P HiKu) described in [32] was used as a reference for this system.

### 2.2.6. Overview of System Parameters

This chapter provides a short overview of the chosen system parameters.

## 2. Methods and Data

	standard	vertical	(back-)tracking	overhead
panel width (E/W dim)	-	1.2m [34]	2.1m [31]	1m [36]
panel length (N/S dim)	4.2m	-	-	-
angle E/W	0°	90°	variable	10° / – 10° [36]
angle N/S	lat. dependent	0°	0°	0°
spacing E/W	-	10m [34]	10m	10m
spacing N/S	7.63m	-	-	-
height (center of panel)	lat. dependent	(1.4m)	1.27m [31]	3.5m [36]
height (clearance)	1m	0.8m [34]	(0.27m)	(~ 3.4m)
number of panels (N/S)	11	1	1	1
number of panels (E/W)	1	9	9	9
total panel area per ha	3360m <sup>2</sup>	864m <sup>2</sup>	1512m <sup>2</sup>	720m <sup>2</sup>
power per panel area	190 W <sub>p</sub> /m <sup>2</sup> [32]	225 W <sub>p</sub> /m <sup>2</sup> [40]	190 W <sub>p</sub> /m <sup>2</sup> [31, 32]	101 W <sub>p</sub> /m <sup>2</sup> [37]
power per field area	639 kW <sub>p</sub> /ha [32]	195 kW <sub>p</sub> /ha [40]	287 kW <sub>p</sub> /ha [31, 32]	72.8 kW <sub>p</sub> /ha [37]

Table 2.1.: System parameters

The parameters in Table 2.1 describe the various PV systems to be simulated. Number of panel columns and rows as well as the power per field area refer to a placement in the standard field layout, with an area of 1ha and a buffer area of 10m on all sides (as shown for the vertical system in Figure 2.15).

The panel tilt in E/W direction  $\beta_{E/W}$  and N/S direction  $\beta_{N/S}$  is defined between 90° and –90°. A 90° tilt describes a panel facing directly east/south, –90° one facing west/north. For fixed systems, tilts are given in Table 2.1. For the standard system, panel tilt is latitude dependent and is listed in A.1. For the tracking and backtracking systems the panel tilt is recalculated for each time step (see 2.4).

The total panel area  $A$  was calculated via formula 2.1.

$$A_{\text{all\_panels}} = m_{\text{panel}} \cdot 80 \cdot n \quad (2.1)$$

Here  $m$  refers to the panel length or width of a given system and  $n$  to the number of rows or columns. Panel rows/columns (depending on the system) have been approximated as one large panel (with a width/length of 80m), neglecting small gaps between panels, for the purpose of simplifying the simulations.

The power per panel area was simply calculated via peak power  $P_{\text{peak}}$  and the panels measurements  $l$  and  $w$  as shown in formula 2.2.

$$\frac{P}{A_{\text{panel}}} = \frac{P_{\text{peak}}}{l \cdot w} \quad (2.2)$$

The power per field area was calculated via multiplication with the total panel area:

$$\frac{P}{A_{\text{field}}} = \frac{P}{A_{\text{panel}}} \cdot m_{\text{Panel}} \cdot 80 \cdot n \quad (2.3)$$

### 2.3. Projection of Sun Beams onto E/W and N/S planes

These variables ( $P_{\text{peak}}$ ,  $l$ ,  $w$ ) were taken from several data sheets describing modules matching the simulated system types [32, 40, 37], these are also cited where used in table 2.1.

## 2.3. Projection of Sun Beams onto E/W and N/S planes

For the calculation of ground- and self-shading (see 2.5) as well as repositioning of tracking and backtracking systems (see 2.4), the angles determining the position of the sun, namely azimuth  $\theta$  and elevation  $\phi$  angles are converted to angles in the E/W and N/S plane. A depiction of this process can be seen in Figure 2.6. The values for azimuth and elevation depending on daytime and location were calculated using the solarposition function from the python module pvlib [26].

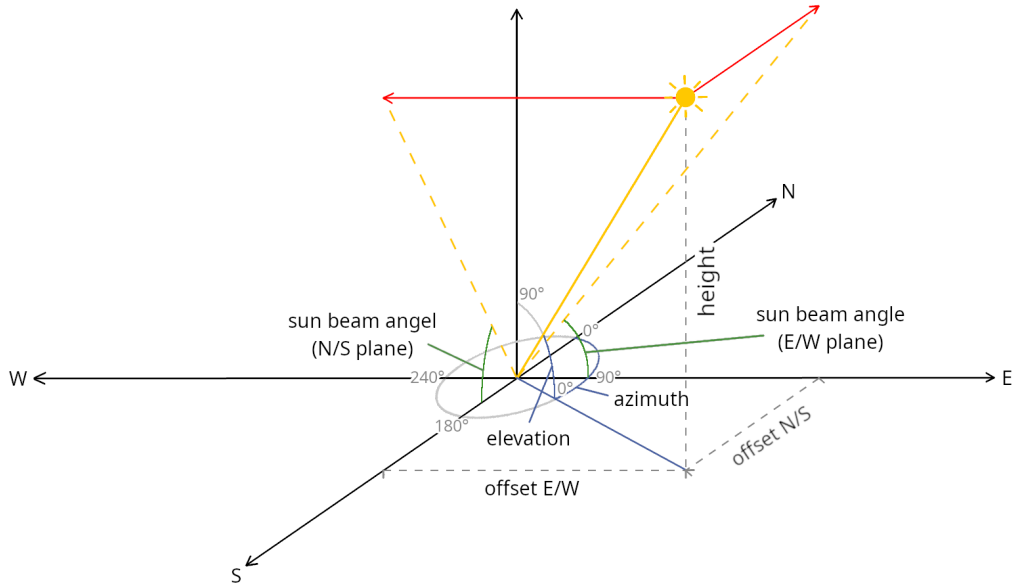


Figure 2.6.: Projection of sun beams onto E/W and N/S planes

In Figure 2.6 the E/W and N/S offsets are the distances between the point of origin in the coordinate system and the location of the sun along the axis representing the E/W and N/S direction respectively. The elevation describes the angle encompassed by the base plane, as defined by the N/S and E/W axis, and the incoming sun beams. The height is the distance of the sun from the base plane along the axis normal to it. All distances are calculated with respect to the sun being located on a unit sphere in  $\mathbb{R}^3$ .

The angles in the E/W plane  $\alpha_{\text{E/W}}$  and N/S plane  $\alpha_{\text{N/S}}$  are calculated as follows:

$$h = \sin\phi \quad (2.4)$$

$$d_{\text{offset, N/S}} = -\cos\theta \cdot \cos\phi \quad (2.5)$$

## 2. Methods and Data

$$d_{\text{offset, E/W}} = \sin\theta \cdot \cos\phi \quad (2.6)$$

$$\alpha_{\text{N/S}} = 90^\circ - \arctan\left(\frac{d_{\text{offset, N/S}}}{h}\right) \quad (2.7)$$

$$\alpha_{\text{E/W}} = 90^\circ - \arctan\left(\frac{d_{\text{offset, E/W}}}{h}\right) \quad (2.8)$$

In these equations  $h$  is the height, and  $d_{\text{offset, N/S}}$  and  $d_{\text{offset, E/W}}$  are the offsets in N/S and E/W direction, as shown and described above.

## 2.4. Repositioning for Tracking and Backtracking Systems

In this section the calculations for the repositioning of the tracking and backtracking systems are going to be described briefly.

### 2.4.1. Tracking System

In the tracking system the panel is repositioned at each time step such that it is orthogonal to the incoming sunbeams projected on the E/W plane.

$$\beta_{\text{E/W}} = 90^\circ - \alpha_{\text{E/W}} \quad (2.9)$$

In equation 2.9  $\beta_{\text{E/W}}$  describes the panel tilt in the E/W plane,  $\alpha_{\text{E/W}}$  the angle of sun beams in the E/W plane.

### 2.4.2. Backtracking System

For the backtracking system the panel is repositioned to be orthogonal to the incoming sunbeams projected on the E/W plane if no self-shading occurs. Otherwise, the panel tilt is set to the nearest angle which avoids self-shading.

In the first step, the tilt is calculated as described in section 2.4.1, then the theoretical width of the projected self-shade is calculated:

$$w_{\text{self-shade}} = w_{\text{panel}} - d_{\text{E/W}} \cdot \sin\alpha_{\text{E/W, mod}} \quad (2.10)$$

$w_{\text{panel}}$  is the width of the panel,  $d_{\text{E/W}}$  the distance between panels in the E/W direction.  $\alpha_{\text{E/W, mod}}$  is the modified angle of the sun in the E/W plane and is determined as follows:  
If  $\alpha_{\text{E/W}} < 90^\circ$ :

$$\alpha_{\text{E/W, mod}} = \alpha_{\text{E/W}} \quad (2.11)$$

If  $\alpha_{\text{E/W}} \geq 90^\circ$ :

$$\alpha_{\text{E/W, mod}} = 180^\circ - \alpha_{\text{E/W}} \quad (2.12)$$

If the resulting self-shade width is smaller than 0 the tilt angle is left unchanged, otherwise the following calculations are made:

If  $\alpha_{\text{E/W}} < 90^\circ$ :

$$\beta_{\text{E/W}} = -\alpha_{\text{E/W}} + \arcsin\left(\frac{d_{\text{E/W}} \cdot \sin\alpha_{\text{E/W}}}{w_{\text{panel}}}\right) \quad (2.13)$$

## 2.5. Shade Projected by Direct Sunlight

Else:

$$\beta_{E/W} = \alpha_{E/W} - \arcsin\left(\frac{d_{E/W} \cdot \sin(180^\circ - \alpha_{E/W})}{w_{\text{panel}}}\right) \quad (2.14)$$

## 2.5. Shade Projected by Direct Sunlight

The following chapters describe how the shaded area on the ground as well as on PV panels was calculated. Simulations were done at  $1^\circ$  steps for latitudes between  $34^\circ\text{N}$  and  $71^\circ\text{N}$  with time intervals of 15 minutes.

### 2.5.1. Ground-Shading

To calculate the shaded area projected on the ground, the position of the four corners of the polygon projected by the PV panel are calculated. All shade polygons were subsequently merged and the total area was calculated. This will be described in detail in the following sections.

To calculate the position of the polygon's corners, incoming direct sunbeams were split into components corresponding to two orthogonal planes, as described in 2.3. For a visualization of how the projected sunbeams were used to calculate ground-shade see Figure 2.7.

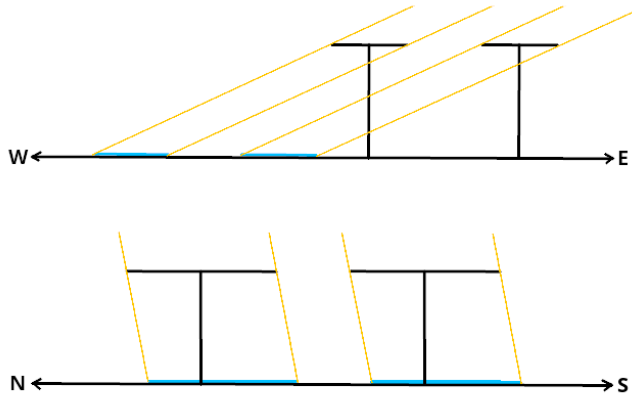


Figure 2.7.: Ground-shading with split sunbeam components

### Calculating height differences between edges

The basis for the calculation of the height differences  $h_{\text{diff}}$  between the panel edges and the base height of the PV panel can be seen in Figure 2.8. The difference is calculated via the following formulas:

$$h_{\text{diff}, W} = \sin(\beta_{E/W}) * \frac{w_{\text{panel}}}{2} \quad (2.15)$$

## 2. Methods and Data

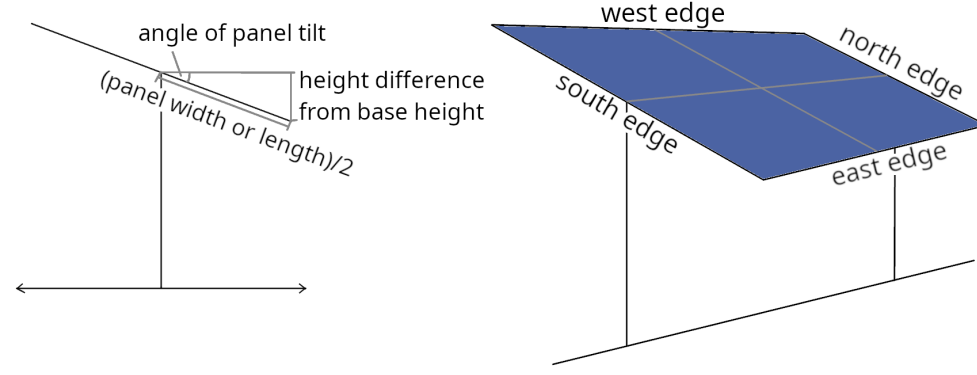


Figure 2.8.: Height difference of edges from base height

$$h_{\text{diff}, E} = -\sin(\beta_{E/W}) * \frac{w_{\text{panel}}}{2} \quad (2.16)$$

$\beta_{E/W}$  is the tilt of the PV panel in the E/W plane for the calculations of height differences of east and west edges.  $w_{\text{panel}}$  is the variable describing the measurement of the panel in E/W direction, also called width here.

$$h_{\text{diff}, N} = \sin(\beta_{N/S}) * \frac{l_{\text{panel}}}{2} \quad (2.17)$$

$$h_{\text{diff}, S} = -\sin(\beta_{N/S}) * \frac{l_{\text{panel}}}{2} \quad (2.18)$$

$\beta_{N/S}$  is the tilt of the PV panel in the N/S plane for the calculations of height differences of south and north edges.  $l_{\text{panel}}$  is the variable describing the measurement of the panel in N/S direction, also called length here.

### Calculating corner heights

The corner heights are calculated by simply adding the height differences of the adjoining edges to the base height. Note that the height differences calculated in equations 2.15, 2.16, 2.17 and 2.18 may be negative.

$$h_{N/E} = h_{\text{base}} + h_{\text{diff}, N} + h_{\text{diff}, E} \quad (2.19)$$

$$h_{N/W} = h_{\text{base}} + h_{\text{diff}, N} + h_{\text{diff}, W} \quad (2.20)$$

$$h_{S/E} = h_{\text{base}} + h_{\text{diff}, S} + h_{\text{diff}, E} \quad (2.21)$$

$$h_{S/W} = h_{\text{base}} + h_{\text{diff}, S} + h_{\text{diff}, W} \quad (2.22)$$

## 2.5. Shade Projected by Direct Sunlight

The variables  $h_{N/E}$ ,  $h_{N/W}$ ,  $h_{S/E}$  and  $h_{S/W}$  stand for the heights of the north-east, north-west, south-east and south-west corners respectively.  $h_{base}$  is the base height of the PV system, meaning the height of the center point of the panel.

### Calculating shade corner positions

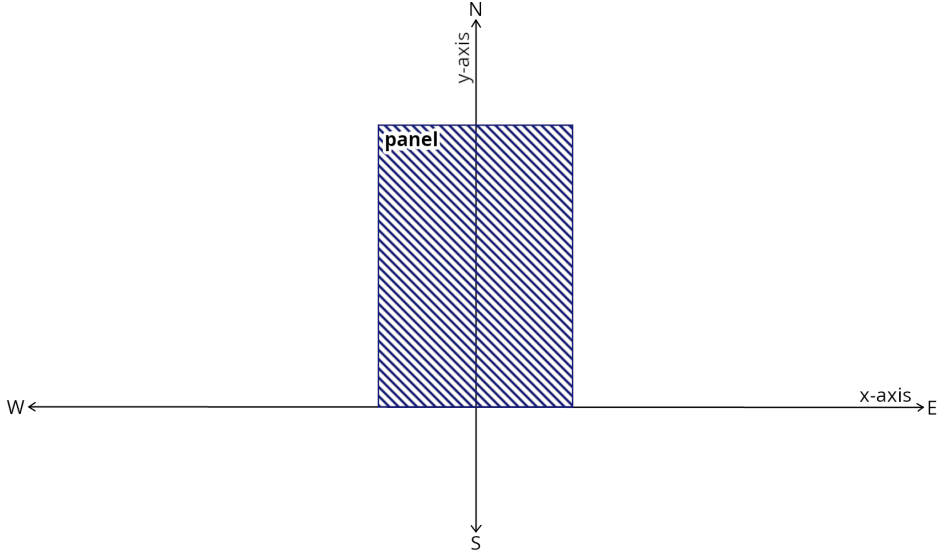


Figure 2.9.: Coordinate system and position of PV panel for N/S aligned systems

In the following section the calculation of the position of the corners of the shade projected on the ground will be discussed. Figure 2.9 shows the coordinate system used for these calculations as well as the position of a PV panel in it.

For systems in which panel rows are aligned with the N/S direction, the x coordinates are calculated as follows. This includes all systems except for the standard system, namely tracking and backtracking, overhead and vertical systems. In these systems the southwesternmost panel is positioned as shown in Figure 2.9, with the middle of the panel sitting at  $x = 0$ .

The x-axis position of the western corners,  $x_{N/W}$  and  $x_{S/W}$ , are determined via the construction shown in Figure 2.10. They are calculated via formulas 2.23 and 2.24.

$$x_{N/W} = -|\cos \beta_{E/W}| \cdot \frac{w_{panel}}{2} - \frac{h_{N/W}}{\tan \alpha_{E/W}} \quad (2.23)$$

$$x_{S/W} = -|\cos \beta_{E/W}| \cdot \frac{w_{panel}}{2} - \frac{h_{S/W}}{\tan \alpha_{E/W}} \quad (2.24)$$

The x-axis position of the eastern corners,  $x_{N/E}$  and  $x_{S/E}$ , are determined via the construction shown in Figure 2.11. They are calculated via formulas 2.25 and 2.26.

## 2. Methods and Data

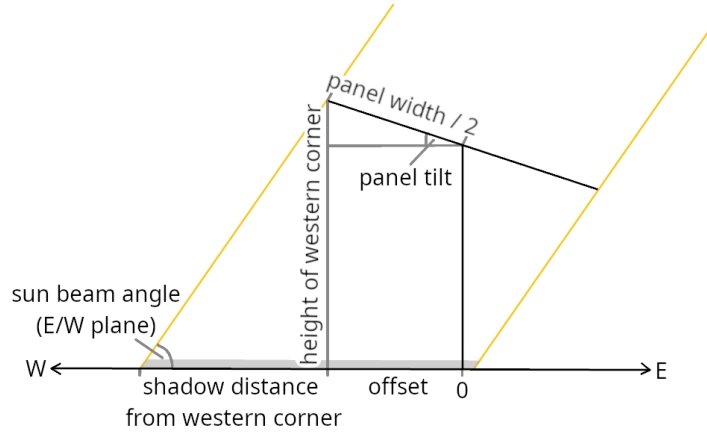


Figure 2.10.: Position of western shade corners

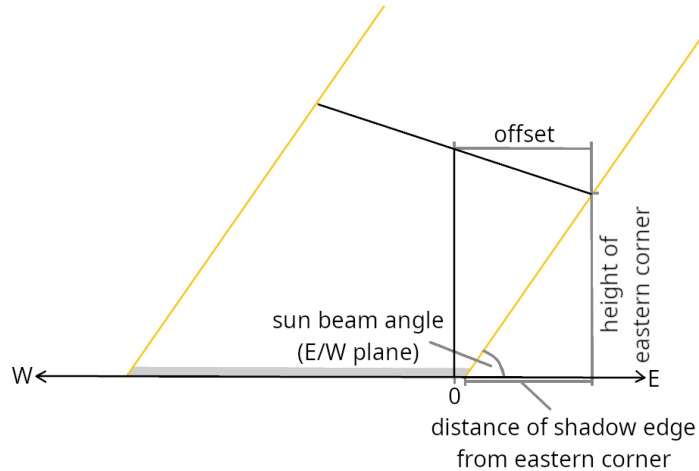


Figure 2.11.: Position of eastern shade corners

$$x_{N/E} = |\cos \beta_{E/W}| \cdot \frac{w_{\text{panel}}}{2} - \frac{h_{N/E}}{\tan \alpha_{E/W}} \quad (2.25)$$

$$x_{S/E} = |\cos \beta_{E/W}| \cdot \frac{w_{\text{panel}}}{2} - \frac{h_{S/E}}{\tan \alpha_{E/W}} \quad (2.26)$$

In these equations  $\beta_{E/W}$  describes the panel tilt in E/W direction,  $\alpha_{E/W}$  the angle of incoming sun beams in the E/W plane. As in the previous section  $w_{\text{panel}}$ ,  $h_{N/W}$ ,  $h_{S/W}$ ,  $h_{N/E}$  and  $h_{S/E}$  stand for the width of the PV panel and the heights of the PV panel's corners respectively.

## 2.5. Shade Projected by Direct Sunlight

In the following, the calculation of x coordinates for systems in which panel rows are aligned with the E/W direction is shown. In this thesis, the only system matching this description is the standard system. The southwesternmost panel is positioned as shown in Figure 2.12, with the middle of the panel sitting at  $x = w_{\text{panel}}/2$ . The x coordinates of the projected shade are calculated as follows.

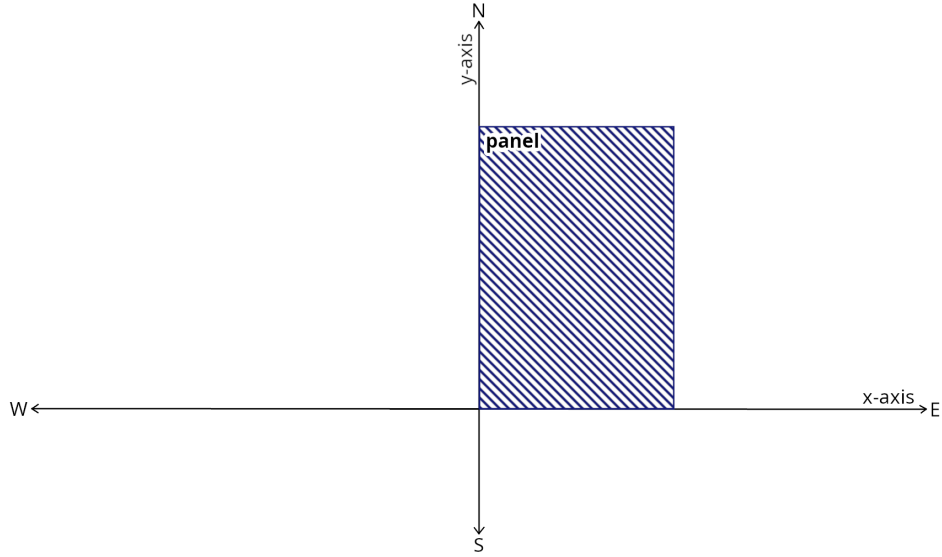


Figure 2.12.: Coordinate system and position of PV panel for E/W aligned systems

The x coordinate positions are calculated as described above, but including the offset necessary for the standard system:

$$x_{\text{N/W}} = \frac{w_{\text{panel}}}{2} - |\cos \beta_{\text{E/W}}| \cdot \frac{w_{\text{panel}}}{2} - \frac{h_{\text{N/W}}}{\tan \alpha_{\text{E/W}}} \quad (2.27)$$

$$x_{\text{S/W}} = \frac{w_{\text{panel}}}{2} - |\cos \beta_{\text{E/W}}| \cdot \frac{w_{\text{panel}}}{2} - \frac{h_{\text{S/W}}}{\tan \alpha_{\text{E/W}}} \quad (2.28)$$

$$x_{\text{N/E}} = \frac{w_{\text{panel}}}{2} + |\cos \beta_{\text{E/W}}| \cdot \frac{w_{\text{panel}}}{2} - \frac{h_{\text{N/E}}}{\tan \alpha_{\text{E/W}}} \quad (2.29)$$

$$x_{\text{S/E}} = \frac{w_{\text{panel}}}{2} + |\cos \beta_{\text{E/W}}| \cdot \frac{w_{\text{panel}}}{2} - \frac{h_{\text{S/E}}}{\tan \alpha_{\text{E/W}}} \quad (2.30)$$

The y-axis position of the northern corners,  $y_{\text{N/W}}$  and  $y_{\text{N/E}}$ , are determined via the construction shown in Figure 2.13. They are calculated via formulas 2.31 and 2.32.

## 2. Methods and Data

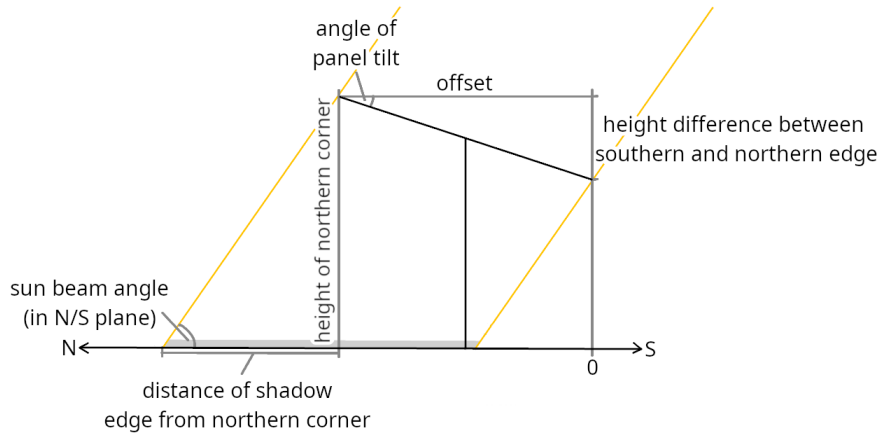


Figure 2.13.: Position of northern shade corners

$$y_{N/W} = \frac{h_{N/W}}{\tan \alpha_{N/S}} + |\cos \beta_{N/S}| \cdot l_{panel} \quad (2.31)$$

$$y_{N/E} = \frac{h_{N/E}}{\tan \alpha_{N/S}} + |\cos \beta_{N/S}| \cdot l_{panel} \quad (2.32)$$

The y-axis position of the southern corners,  $y_{S/W}$  and  $y_{S/E}$ , are determined via the construction shown in Figure 2.14. They are calculated via formulas 2.33 and 2.34.

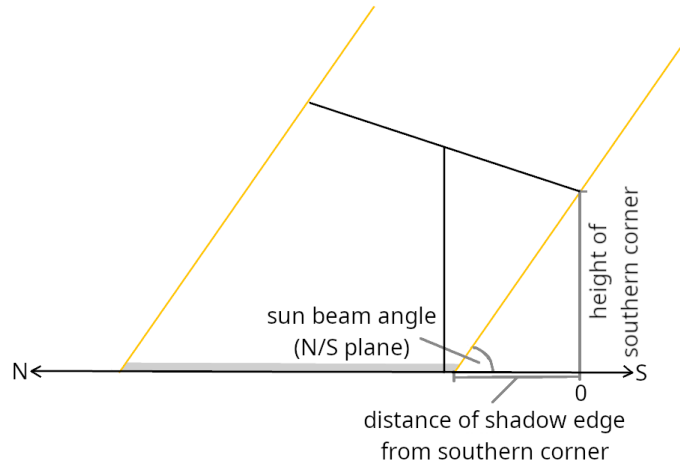


Figure 2.14.: Position of southern shade corners

$$y_{S/W} = \frac{h_{S/W}}{\tan \alpha_{N/S}} \quad (2.33)$$

## 2.5. Shade Projected by Direct Sunlight

$$y_{S/E} = \frac{h_{S/E}}{\tan \alpha_{N/S}} \quad (2.34)$$

In the equations 2.31, 2.32, 2.33 and 2.34,  $\beta_{N/S}$  describes the panel tilt in N/S direction,  $\alpha_{N/S}$  the angle of incoming sun beams in the N/S plane. As in the previous section  $l_{\text{panel}}$ ,  $h_{N/W}$ ,  $h_{S/W}$ ,  $h_{N/E}$  and  $h_{S/E}$  stand for the length of the PV panel and the heights of the PV panel's corners respectively.

### Calculating total shade on field

In the final step of the calculation, the shade cast by a single panel is turned into a polygon using the previously calculated shade corners.

First, a copy of the polygon is then added for all simulated PV panels, with the distances between shadow polygons being the distances between PV panels. In this context the distances refer to the distances between center points of both shadows and panels.

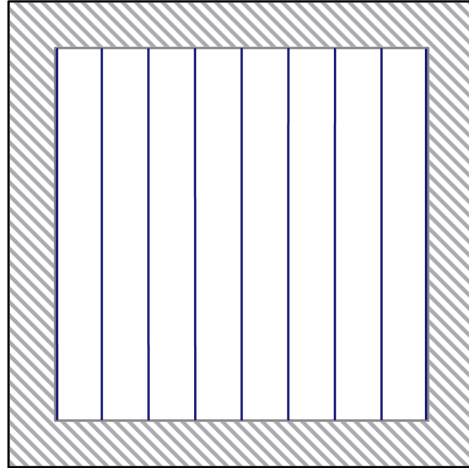


Figure 2.15.: Field layout with vertical PV panels

Second, the field limits are defined. In this thesis a standard field is defined as a 100 by 100 meter square, an area of one hectare. This includes a buffer area with a width of 10 meters. An illustration of this can be seen in Figure 2.15, the hatched area represents the buffer, the dark blue lines columns of vertical PV panels.

In the last step, the intersection area of the shade polygons with the field is calculated. This intersection is expressed in percent of the total field area. All calculations in relation to the created polygons were done using the python module shapely [41].

## 2. Methods and Data

### 2.5.2. Self-Shading

In the following section, the approach to calculating the self-shaded area in the agrivoltaic systems will be discussed. Separate methods are used for tracking, vertical, standard and overhead systems. The backtracking system is excluded here, since the panel tilt in that system is set to avoid self-shading.

#### Tracking System

Firstly, the sun angle in the E/W plane and the azimuth are modified. These modifications are made, so further calculations can be done without case distinctions. The sun angle in the E/W plane  $\alpha_{E/W, \text{mod}}$  is changed to simulate the sun always coming from the east with the following formulas:

If  $\alpha_{E/W} < 90^\circ$ :

$$\alpha_{E/W, \text{mod}} = \alpha_{E/W} \quad (2.35)$$

If  $\alpha_{E/W} \geq 90^\circ$ :

$$\alpha_{E/W, \text{mod}} = 180 - \alpha_{E/W} \quad (2.36)$$

The azimuth  $\theta_{\text{mod}}$  is modified to give the (minimal) angle off the meridian, putting it in the north-east quadrant:

If  $\theta \leq 90^\circ$ :

$$\theta_{\text{mod}} = \theta \quad (2.37)$$

If  $\theta > 90^\circ$  and  $\theta \leq 180^\circ$ :

$$\theta_{\text{mod}} = 180^\circ - \theta \quad (2.38)$$

If  $\theta > 180^\circ$  and  $\theta \leq 270^\circ$ :

$$\theta_{\text{mod}} = \theta - 180^\circ \quad (2.39)$$

If  $\theta > 270^\circ$ :

$$\theta_{\text{mod}} = 360^\circ - \theta \quad (2.40)$$

Next, the width of the shade projected on the neighbouring panel  $w_{\text{shade}}$  is calculated as described in formula 2.41. A visual representation is shown in Figure 2.16.

$$w_{\text{shade}} = w_{\text{panel}} - \sin \alpha_{E/W, \text{mod}} \cdot d_{E/W} \quad (2.41)$$

In this equation  $w_{\text{panel}}$  is the width of the PV panel,  $\alpha_{E/W, \text{mod}}$  the angle between sunbeams and the ground projected on the E/W plane and  $d_{E/W}$  the distance between PV panels.

The self-shading offset in N/S direction is calculated via the distance between the top edge of the illuminated panel and the top edge of the shaded panel from a bird's-eye view  $d_{\text{shade, panel}}$  and the angle off center  $\theta_{\text{mod}}$  as shown in Figure 2.17.

$$d_{\text{shade, panel}} = d_{E/W} - (w_{\text{panel}} - w_{\text{shade}}) \cdot \cos \beta_{E/W} \quad (2.42)$$

$$l_{\text{offset}} = \tan (90^\circ - \theta_{\text{mod}}) \cdot d_{\text{shade, panel}} \quad (2.43)$$

## 2.5. Shade Projected by Direct Sunlight

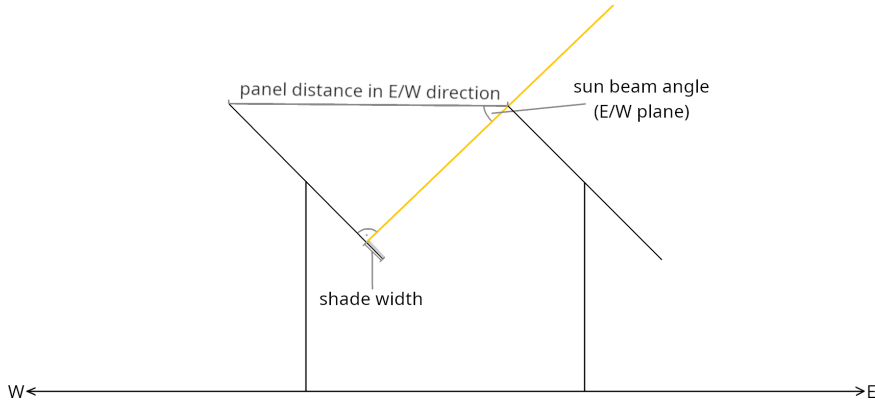


Figure 2.16.: Shade width in tracking system

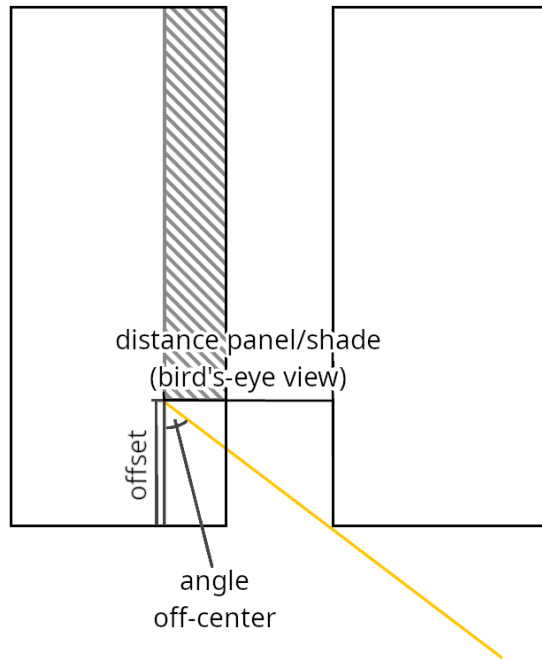


Figure 2.17.: Offset calculation

The shaded panel length  $l_{\text{shade}}$  is then calculated from the offset:

$$l_{\text{shade}} = (\text{nmb}_{\text{N/S}} - 1) \cdot d_{\text{N/S}} + l_{\text{panel}} - l_{\text{offset}} \quad (2.44)$$

A visual representation of these parameters can be seen in Figure 2.18.

In the next step the number of fully shaded panels  $\text{nmb}_{\text{fully shaded}}$  is calculated from the shaded panel length. In this context the number of fully shaded panels refers to the

## 2. Methods and Data

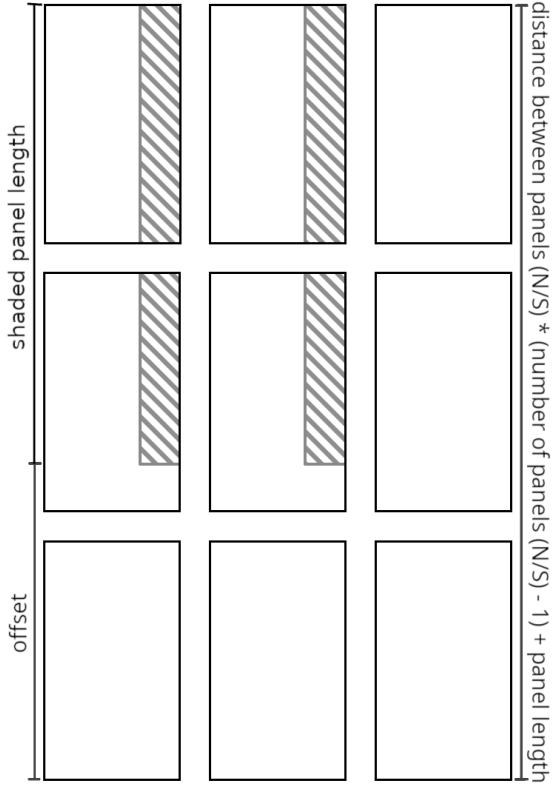


Figure 2.18.: Offset and shade length in tracking system

panels with self-shade extending their full length, meaning they are not affected by the previously calculated offset. This description would apply to the first two panels in the top row in Figure 2.18.

If  $l_{\text{shade}} < l_{\text{panel}}$ :

$$nmb_{\text{fully shaded}} = 0 \quad (2.45)$$

Else:

$$nmb_{\text{fully shaded}} = (\text{Floor}(\frac{l_{\text{shade}} - l_{\text{panel}}}{d_{\text{N/S}}}) + 1) \cdot (nmb_{\text{E/W}} - 1) \quad (2.46)$$

This number is used to calculate the regular shade  $A_{\text{self-shade, regular}}$ :

$$A_{\text{self-shade, regular}} = nmb_{\text{fully shaded}} \cdot w_{\text{shade}} \cdot l_{\text{panel}} \quad (2.47)$$

Then the shaded area on irregularly shaded panels (e.g. first two panels in the second row in Figure 2.18) is calculated.

Should the offset end between panels or all panels be fully shaded, the irregularly shaded area is set to zero:

## 2.5. Shade Projected by Direct Sunlight

If  $l_{\text{offset}} \bmod d_{\text{N/S}} > l_{\text{panel}}$  or  $nmb_{\text{fully shaded}} = nmb_{\text{N/S}} \cdot (nmb_{\text{E/W}} - 1)$ :

$$A_{\text{self-shade, irregular}} = 0 \quad (2.48)$$

Else the following calculation is made:

$$A_{\text{self-shade, irregular}} = w_{\text{shade}} \cdot (l_{\text{panel}} - (l_{\text{offset}} \bmod d_{\text{N/S}})) \cdot (nmb_{\text{E/W}} - 1) \quad (2.49)$$

Lastly the total self-shaded area is determined by adding the previous two results:

$$A_{\text{self-shade, total}} = A_{\text{self-shade, regular}} + A_{\text{self-shade, irregular}} \quad (2.50)$$

The result is returned in percent of the total panel area:

$$A_{\text{self-shade, relative}} = \frac{A_{\text{self-shade, total}}}{nmb_{\text{E/W}} \cdot nmb_{\text{N/S}} \cdot w_{\text{panel}} \cdot l_{\text{panel}}} \quad (2.51)$$

## Vertical System

Self-shading in the vertical system is calculated in largely the same way as in the tracking system with the exception of the shade width (2.41). In the vertical system it is calculated via the following formula:

$$w_{\text{shade}} = w_{\text{panel}} - \tan \alpha_{\text{E/W}} \bmod \cdot d_{\text{E/W}} \quad (2.52)$$

A visual representation of this can be seen in Figure 2.19.

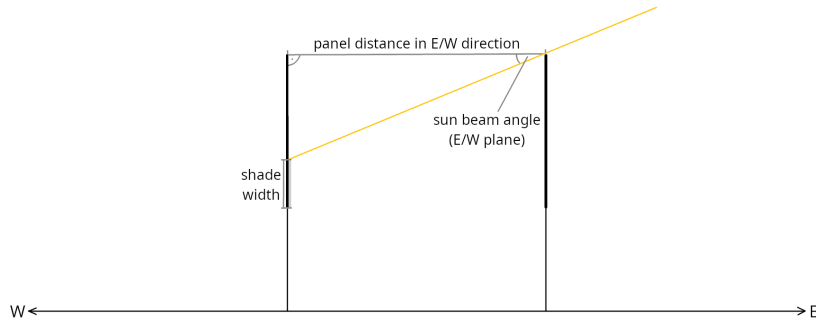


Figure 2.19.: Shade width in vertical system

## 2. Methods and Data

### Standard System

For this system the first step is checking the sun angle in the N/S plane  $\alpha_{N/S}$ . If the angle is in the area shaded in orange in Figure 2.20, the self-shade is set to 0%, since no self-shading is possible at these angles. If it is in the area shaded in blue in Figure 2.20, self-shade is set to 100% as the sun will be hitting the back of the panels at these angles. Otherwise  $\alpha_{N/S}$  is left unmodified for further calculations.

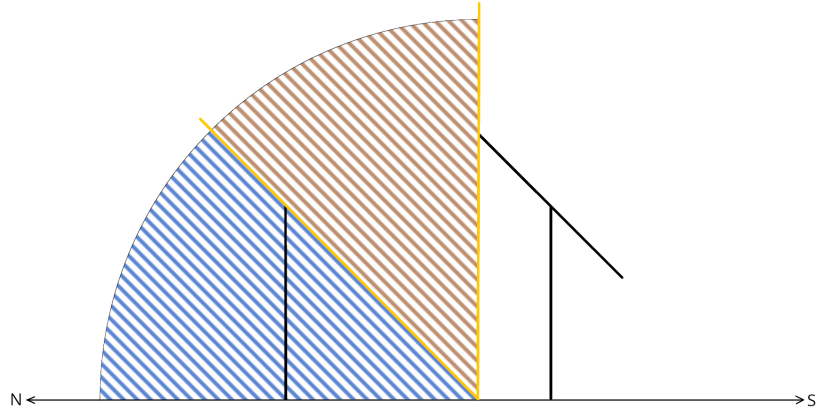


Figure 2.20.: Sun angles in N/S plane for standard system

For this system the azimuth is also modified similarly to the previous cases to avoid case distinctions:

If  $\theta \leq 90^\circ$ :

$$\theta_{\text{mod}} = \theta \quad (2.53)$$

If  $\theta > 90^\circ$  and  $\theta \leq 180^\circ$ :

$$\theta_{\text{mod}} = 180^\circ - \theta \quad (2.54)$$

If  $\theta > 180^\circ$  and  $\theta \leq 270^\circ$ :

$$\theta_{\text{mod}} = \theta - 180^\circ \quad (2.55)$$

If  $\theta > 270^\circ$ :

$$\theta_{\text{mod}} = 360^\circ - \theta \quad (2.56)$$

Next, the width of the shade projected on the neighbouring panel  $w_{\text{shade}}$  is calculated as described below. A visual representation is shown in Figure 2.21.

$$\gamma = 180^\circ - \alpha_{N/S} + \beta_{N/S} \quad (2.57)$$

$$a = \frac{d_{N/S}}{\sin \gamma} \cdot \sin \alpha_{N/S} \quad (2.58)$$

$$w_{\text{shade}} = l_{\text{panel}} - a \quad (2.59)$$

## 2.5. Shade Projected by Direct Sunlight

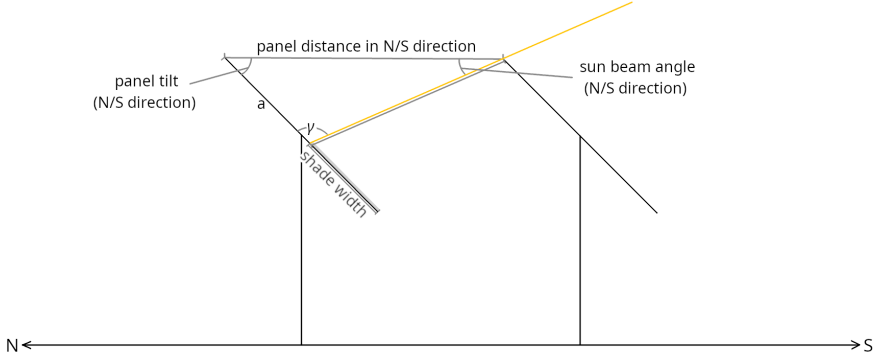


Figure 2.21.: Shade width in standard system

In this equation,  $l_{\text{panel}}$  is the length of the PV panel,  $\alpha_{\text{N/S}}$  the angle between sunbeams and the ground projected on the N/S plane,  $\beta_{\text{N/S}}$  is the angle of the panel in the N/S plane and  $d_{\text{N/S}}$  the distance between PV panels in the N/S direction.

The self-shading offset in E/W direction is calculated via the distance between the top edge of the illuminated panel and the top edge of the shaded panel from a bird's-eye view  $d_{\text{shade, panel}}$  and the angle off center  $\theta_{\text{mod}}$  as shown in Figure 2.17.

$$d_{\text{shade, panel}} = d_{\text{N/S}} - (l_{\text{panel}} - w_{\text{shade}}) \cdot \cos \beta_{\text{N/S}} \quad (2.60)$$

$$l_{\text{offset}} = \tan \theta_{\text{mod}} \cdot d_{\text{shade, panel}} \quad (2.61)$$

The shaded panel length  $l_{\text{shade}}$  is then calculated from the offset:

$$l_{\text{shade}} = (nmb_{\text{E/W}} - 1) \cdot d_{\text{E/W}} + w_{\text{panel}} - l_{\text{offset}} \quad (2.62)$$

A visual representation of these parameters can be seen in Figure 2.22.

In the next step the number of fully shaded panels  $nmb_{\text{fully shaded}}$  is calculated from the shaded panel length. In this context the number of fully shaded panels refers to the panels with self-shade extending their full length, meaning they are not affected by the previously calculated offset. This description would apply to the top two panels on the right side in Figure 2.22.

If  $l_{\text{shade}} < w_{\text{panel}}$ :

$$nmb_{\text{fully shaded}} = 0 \quad (2.63)$$

Else:

$$nmb_{\text{fully shaded}} = (\text{Floor}(\frac{l_{\text{shade}} - w_{\text{panel}}}{d_{\text{E/W}}}) + 1) \cdot (nmb_{\text{N/S}} - 1) \quad (2.64)$$

This number is used to calculate the regular shade  $A_{\text{self-shade, regular}}$ :

$$A_{\text{self-shade, regular}} = nmb_{\text{fully shaded}} \cdot w_{\text{shade}} \cdot w_{\text{panel}} \quad (2.65)$$

## 2. Methods and Data

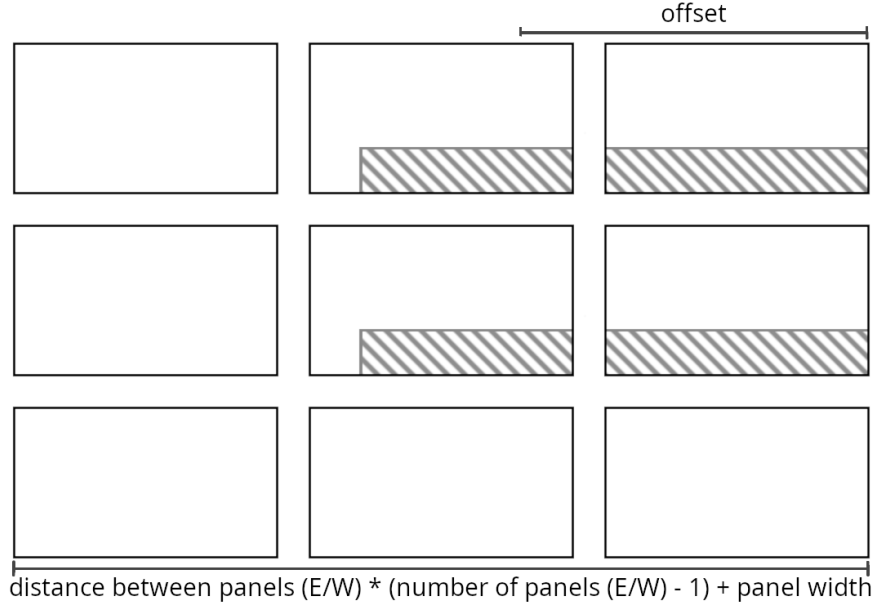


Figure 2.22.: Offset and shade length in standard system

Then the shaded area on irregularly shaded panels (e.g. top two panels in the middle column in Figure 2.22) is calculated. Should the offset end between panels or all panels be fully shaded, the irregularly shaded area is set to zero: If  $l_{\text{offset}} \bmod d_{\text{E/W}} > w_{\text{panel}}$  or  $nmb_{\text{fully shaded}} = nmb_{\text{E/W}} \cdot (nmb_{\text{N/S}} - 1)$ :

$$A_{\text{self-shade, irregular}} = 0 \quad (2.66)$$

Else the following calculation is made:

$$A_{\text{self-shade, irregular}} = w_{\text{shade}} \cdot (w_{\text{panel}} - (l_{\text{offset}} \bmod d_{\text{E/W}})) \cdot (nmb_{\text{N/S}} - 1) \quad (2.67)$$

Lastly the total self-shaded area is determined by adding the previous two results:

$$A_{\text{self-shade, total}} = A_{\text{self-shade, regular}} + A_{\text{self-shade, irregular}} \quad (2.68)$$

The result is returned in percent of the total panel area:

$$A_{\text{self-shade, relative}} = \frac{A_{\text{self-shade, total}}}{nmb_{\text{E/W}} \cdot nmb_{\text{N/S}} \cdot w_{\text{panel}} \cdot l_{\text{panel}}} \quad (2.69)$$

### Overhead System

In the first step the sun angle in the E/W plane  $\alpha_{\text{N/S}}$  is checked. If the angle is in the area shaded in orange in Figure 2.23, the self-shade is set to 0%, since no self-shading is possible at these angles. If it is in the area shaded in blue in Figure 2.23, self-shade is

## 2.5. Shade Projected by Direct Sunlight

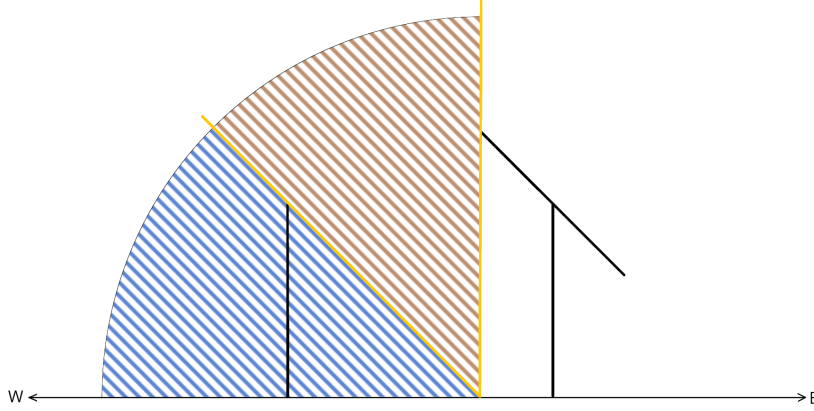


Figure 2.23.: Sun angles in E/W plane for overhead system

set to 100% as the sun will be hitting the back of the panels at these angles. Otherwise  $\alpha_{E/W}$  is left unmodified for further calculations.

For this system the azimuth is also modified similarly to the previous cases to avoid later case distinctions:

If  $\theta \leq 90^\circ$ :

$$\theta_{\text{mod}} = \theta \quad (2.70)$$

If  $\theta > 90^\circ$  and  $\theta \leq 180^\circ$ :

$$\theta_{\text{mod}} = 180^\circ - \theta \quad (2.71)$$

If  $\theta > 180^\circ$  and  $\theta \leq 270^\circ$ :

$$\theta_{\text{mod}} = \theta - 180^\circ \quad (2.72)$$

If  $\theta > 270^\circ$ :

$$\theta_{\text{mod}} = 360^\circ - \theta \quad (2.73)$$

Next, the width of the shade projected on the neighbouring panel  $w_{\text{shade}}$  is calculated as described below. A visual representation is shown in Figure 2.24.

$$\gamma = 180^\circ - \alpha_{E/W} + \beta_{E/W} \quad (2.74)$$

$$a = \frac{d_{E/W}}{\sin \gamma} \cdot \sin \alpha_{E/W} \quad (2.75)$$

$$w_{\text{shade}} = w_{\text{panel}} - a \quad (2.76)$$

In this equation  $w_{\text{panel}}$  is the width of the PV panel,  $\alpha_{E/W}$  the angle between sunbeams and the ground projected on the E/W plane,  $\beta_{E/W}$  is the angle of the panel in the E/W plane and  $d_{E/W}$  the distance between PV panels in the E/W direction.

## 2. Methods and Data

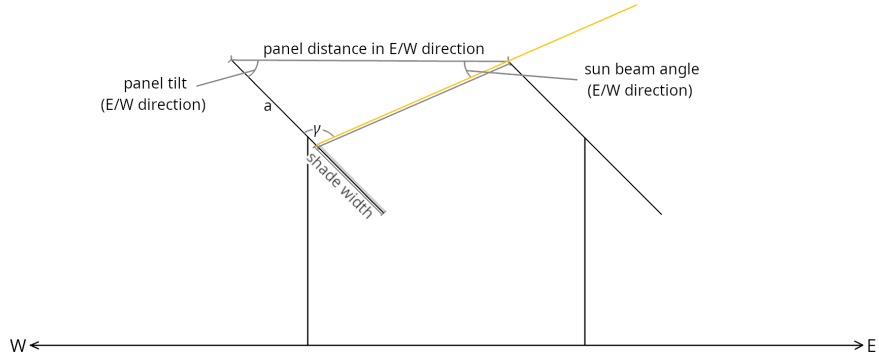


Figure 2.24.: Shade width in overhead system

The self-shading offset in N/S direction is calculated via the distance between the top edge of the illuminated panel and the top edge of the shaded panel from a bird's-eye view  $d_{\text{shade, panel}}$  and the angle off center  $\theta_{\text{mod}}$  as shown in Figure 2.17.

$$d_{\text{shade, panel}} = d_{\text{E/W}} - (w_{\text{panel}} - w_{\text{shade}}) \cdot \cos \beta_{\text{E/W}} \quad (2.77)$$

$$l_{\text{offset}} = \tan(90^\circ - \theta_{\text{mod}}) \cdot d_{\text{shade, panel}} \quad (2.78)$$

The shaded panel length  $l_{\text{shade}}$  is then calculated from the offset:

$$l_{\text{shade}} = (nmb_{\text{N/S}} - 1) \cdot d_{\text{N/S}} + l_{\text{panel}} - l_{\text{offset}} \quad (2.79)$$

A visual representation of these parameters can be seen in Figure 2.25.

In the next step the number of fully shaded panels  $nmb_{\text{fully shaded}}$  is calculated from the shaded panel length. In this context the number of fully shaded panels refers to the panels with self-shade extending their full length, meaning they are not affected by the previously calculated offset. This description would apply to the first two panels in the top row in Figure 2.25.

If  $l_{\text{shade}} < l_{\text{panel}}$ :

$$nmb_{\text{fully shaded}} = 0 \quad (2.80)$$

Else:

$$nmb_{\text{fully shaded}} = (\text{Floor}\left(\frac{l_{\text{shade}} - l_{\text{panel}}}{d_{\text{N/S}}}\right) + 1) \cdot (nmb_{\text{E/W}} - 1) \quad (2.81)$$

This number is used to calculate the regular shade  $A_{\text{self-shade, regular}}$ :

$$A_{\text{self-shade, regular}} = nmb_{\text{fully shaded}} \cdot w_{\text{shade}} \cdot l_{\text{panel}} \quad (2.82)$$

Then the shaded area on irregularly shaded panels (e.g. first two panels in the middle row in Figure 2.25) is calculated. Should the offset end between panels or all panels be

## 2.5. Shade Projected by Direct Sunlight

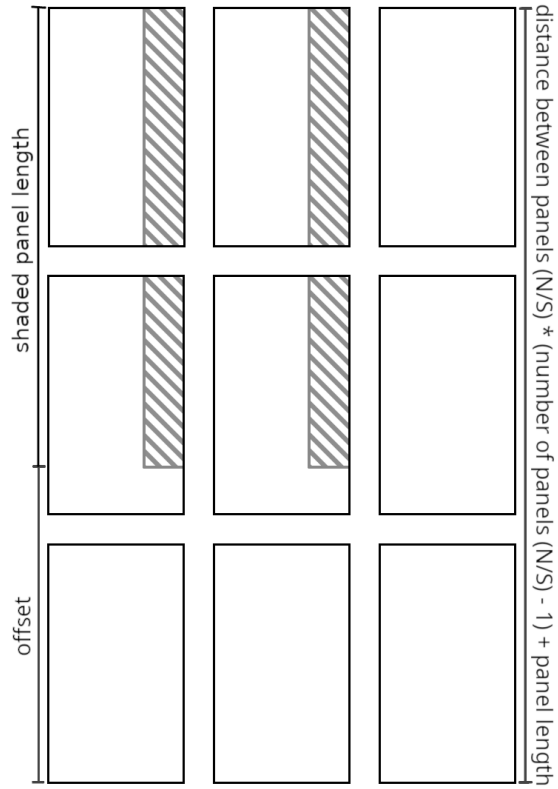


Figure 2.25.: Offset and shade length in overhead system

fully shaded, the irregularly shaded area is set to zero: If  $l_{\text{offset}} \bmod d_{N/S} > l_{\text{panel}}$  or  $nmb_{\text{fully shaded}} = nmb_{N/S} \cdot (nmb_{E/W} - 1)$ :

$$A_{\text{self-shade, irregular}} = 0 \quad (2.83)$$

Else the following calculation is made:

$$A_{\text{self-shade, irregular}} = w_{\text{shade}} \cdot (l_{\text{panel}} - (l_{\text{offset}} \bmod d_{N/S})) \cdot (nmb_{E/W} - 1) \quad (2.84)$$

Lastly the total self-shaded area is determined by adding the previous two results:

$$A_{\text{self-shade, total}} = A_{\text{self-shade, regular}} + A_{\text{self-shade, irregular}} \quad (2.85)$$

The result is returned in percent of the total panel area:

$$A_{\text{self-shade, relative}} = \frac{A_{\text{self-shade, total}}}{nmb_{E/W} \cdot nmb_{N/S} \cdot w_{\text{panel}} \cdot l_{\text{panel}}} \quad (2.86)$$

## 2. Methods and Data

### 2.5.3. Percentage of Time Shaded

In addition to the calculation of the percentage of the shaded field/panel area, the model was used to determine how ground-shade is distributed on the simulated field area. The data was retrieved as a yearly average for all systems and relevant latitudes.

To determine shade distribution a grid of points with a distance of 1m spanning the entire field is generated (see Figure 2.26). For each time step at which the sun is above the horizon, the ground shading is calculated. The polygons created for this calculation are then used to check which points in the aforementioned grid are in the shaded portions of the field at this time step. In the array describing these points one is added to a counter, should the point fall within the shaded areas.

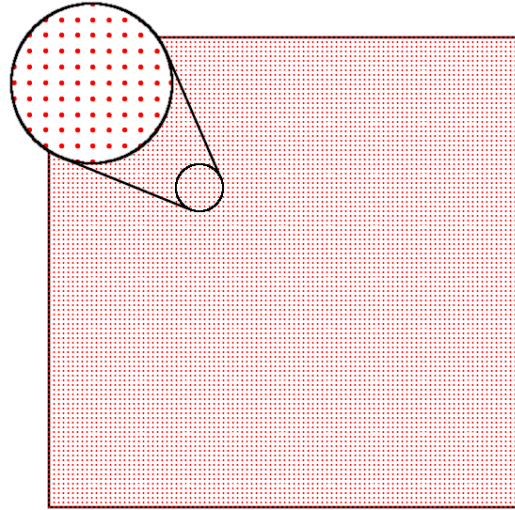


Figure 2.26.: Grid layout for percentage of time shaded calculations

For this thesis, the counts were tallied over one year. Lastly the resulting numbers were divided by the total number of relevant time-steps, in this case being those with a solar elevation greater than  $0^\circ$ .

# 3. Results

This section presents the results of analysing the generated datasets with respect to several aspects, including illuminated time, ground- and panel-shading. A particular focus of this is to show differences in the previously established agrivoltaic systems.

## 3.1. Average Shading

In the following, the average amount of ground- and self-shading is shown for all simulated systems. The results are given depending on latitude, daytime and time of the year. Additionally, a comparison is made between results under the inclusion of horizon data and those without.

### 3.1.1. Average Shading Depending on Latitude

Figures 3.1 and 3.2 depict ground- and self-shading in all systems over the simulated latitudes. Figure 3.1 shows averaged shading values including nighttime hours, while in Figure 3.2 only values calculated during daytime hours are included. Horizon data has not been included in these graphics. In this context daytime refers to times at which solar elevation is larger than  $0^\circ$ .

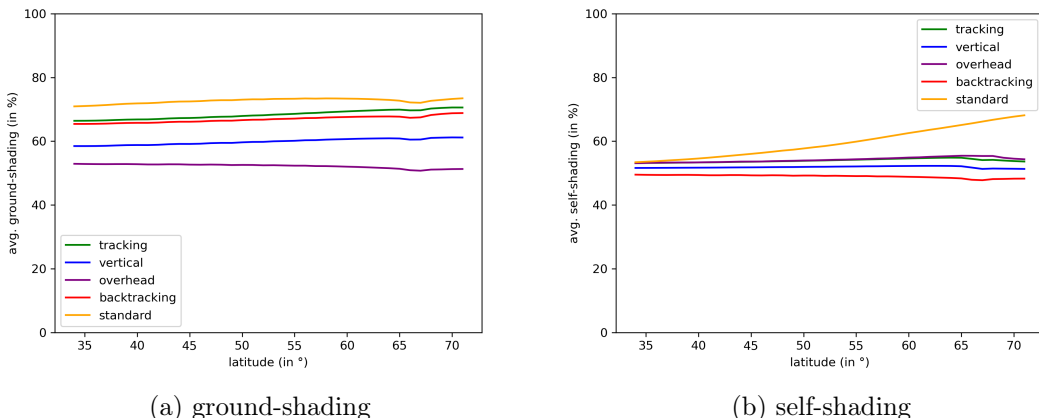


Figure 3.1.: Shading over latitudes - including nighttime

### 3. Results

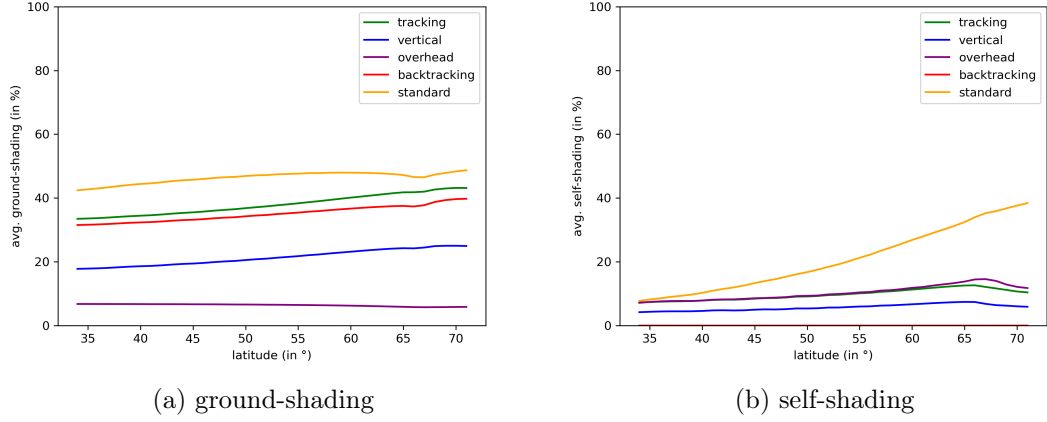


Figure 3.2.: Shading over latitudes - daytime

Overall, results shown here match expectations, with a slight increase in shading at higher latitudes for most systems. The standard system exhibits the largest change in self-shading, this is presumably due to the static N/S spacing (described in 2.2.6) having a strong effect on self-shading.

The dip in averaged ground- and self-shading around a latitude of approximately 65°N matches the location of the polar circle at 66°33'N. The irregularity around this point can be explained by the combined effect of polar day and night at these high latitudes and the fixed borders of the field. The consistently low elevation of the sun leads to a high portion of the total projected ground-shade being located outside the simulated field area. This leads to slightly decreased numbers in the model.

A similar trend can be seen in self-shading results in north/south aligned systems. Here the increase in self-shading from lower solar elevation is offset by the sun being located closer to the south direction. The latter leads to a larger offset, as defined in 2.5.2, and thus a smaller portion of shade being projected on panels.

A close look at the development of self- and ground-shading dependent on latitude reveals an irregular development in average shade where it resembles the shape of a stair function, sometimes even presenting a slight decline at higher latitudes. This presumably occurs due to edge effects resulting from the defined standard field boundaries as well as the size of timesteps used in the simulations. With the sun at a relatively higher elevation at a lower latitude the total projected ground-shaded area is smaller, but the lower elevation of the sun at higher latitudes causes a greater portion of the ground-shade to be projected outside of the predefined field area at a certain timestep. In combination with the simulation being done at 15 min intervals, this likely causes the effect shown in 3.3. A similar timestep dependent effect causes the same in self-shading data. At shorter time intervals this effect vanishes, see Figure 3.3.

### 3.1. Average Shading

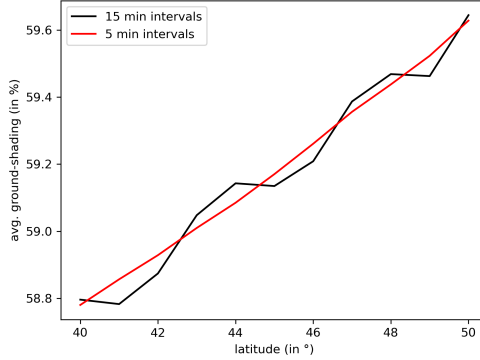


Figure 3.3.: Comparison of calculated ground-shading with different time intervals

From Figure 3.1a it can be concluded that ground-shading is by far the lowest in the simulated overhead system. Successive higher ground-shading is projected by the vertical, backtracking, tracking and standard systems. Results for the tracking and backtracking systems are similar, the gap resulting from the differing panel orientation in the early morning and late in the evening, where the effect of self-shading is present.

The increased self-shading in the overhead system when compared to the tracking and vertical systems can be explained through the way self-shading was defined in this system, whereby a low elevation of the sun in the west results in self-shade being set to 100%. For details see 2.5.2. The effect of this is particularly visible at high latitudes, where a low solar elevation is more common.

Lastly, the lowest self-shading can be observed in the backtracking system. In this system, self shading is zero during daytime by definition, as the panels are positioned accordingly.

#### 3.1.2. Average Shading Depending on Daytime

In Figures 3.4a and 3.4b average ground- and self-shading in all systems is plotted depending on daytime. Horizon data is excluded here.

The overall trend in these figures is as expected, with a dip in shading during daytime hours. As before, shading in the standard system is generally higher, presumably due to the chosen spacing.

Regarding ground-shading, the tracking and backtracking systems yield very similar results, with more differences closer to nighttime. This is what can be predicted from the positioning in these systems. Self-shading occurs mostly close to sunrise and sunset, as such positioning in the backtracking system differs from the tracking system at these times, leading to differences in ground-shading.

Further, Figure 3.4a shows asymmetrically distributed ground-shading for the overhead system. Specifically, there is higher ground-shading in the first half of the day compared to the second. This is due to the panels in this system being fixed at a slight tilt facing east.

### 3. Results

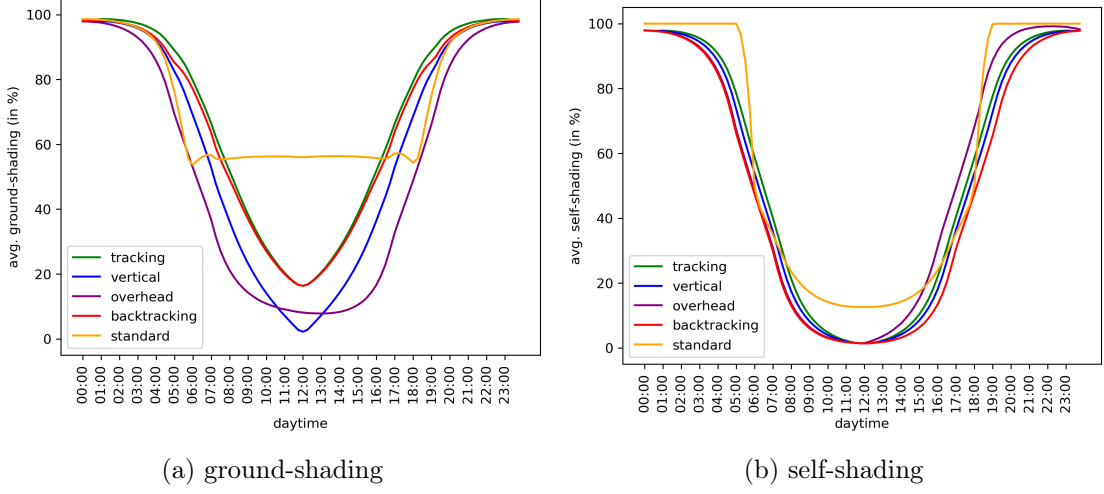


Figure 3.4.: Shading by daytime

The vertical system shows the lowest dip in ground-shading at midday, which results from the fixed vertical positioning in this system. The panels project little shade when the sun is positioned near the south direction. Closer to sunrise and sunset ground-shading values resemble those in the tracking and backtracking systems, due to similar positioning of the latter at those times.

The shape of the curve describing the standard system in 3.4a can be explained by taking a look at Figure A.4a, which shows the how ground-shading develops at different times of the year. During winter a shape similar to other systems is present, albeit with increased ground-shading values. During summer months, ground shading dips in the morning and evening, with an increase during midday. The first is caused by the sun being located to the east/west illuminating the field from the side, only slightly inhibited by photovoltaic panels. Closer to midday, when the sun moves closer to the South position, a higher portion of light is blocked off by the panels in the east/west aligned system. This should be expected in the standard system, since it is typically meant to optimise for electricity generation. The peculiar shape of the average curve, also seen in 3.4a, is caused by the aggregation of results across the whole year.

Self-shading is similar across systems, with the most notable deviations being that of the standard system explained before, and that of the overhead system. The asymmetry can once again be explained by the east-facing tilt of the panels.

Comparing the daily course of shading at different times of the year yields the result shown in Figure 3.5. Figure 3.5 depicts this comparison for the vertical system. In other setups results are similar (see A.2).

Looking at the differences in shading at different times of the year, results match with changes in day-length, with the exception of the standard system described above. During summer average shading is generally lower, during the winter it is higher. Around morning and evening there are some irregularities, which are particularly noticeable in the lines

### 3.1. Average Shading

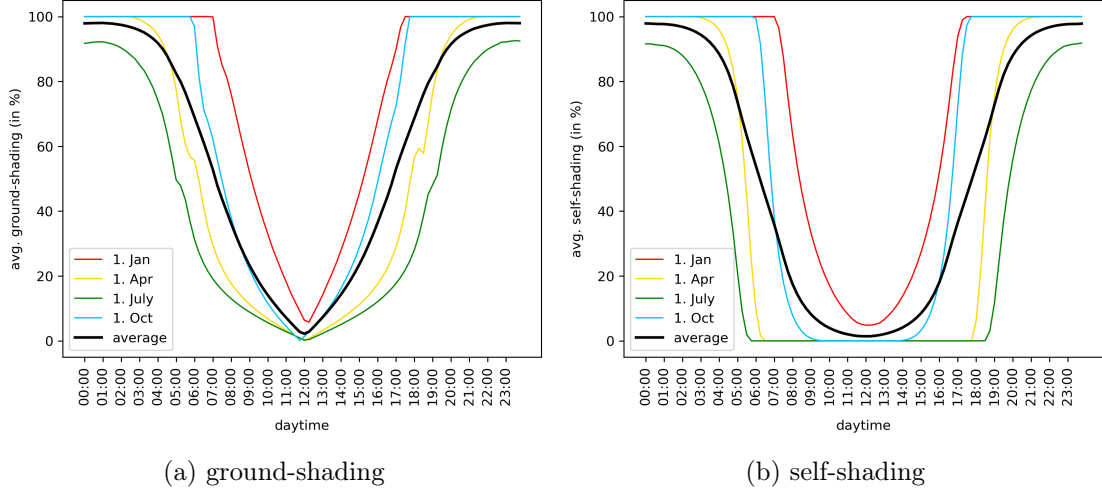


Figure 3.5.: Shading by daytime at different times of the year in vertical system

representing the 1<sup>st</sup> of April and July in Figure 3.5a. These can be explained by the effect of the chosen field borders, similar to what was explained in 3.1.1. At these times the shade projected by the sun is generally high, but because of the low elevation of the sun, a large portion of it is projected outside the predefined field area. As the elevation of the sun increases the proportion of the shade projected on the field increases briefly before falling again, due to the total shaded area decreasing.

Figures 3.6a and 3.6b compare the average daily course of ground- and self-shading under the inclusion/exclusion of horizon data. For these graphs data, which does not factor in horizons, has been weighted to match the distribution latitudes present in the mastergrid.

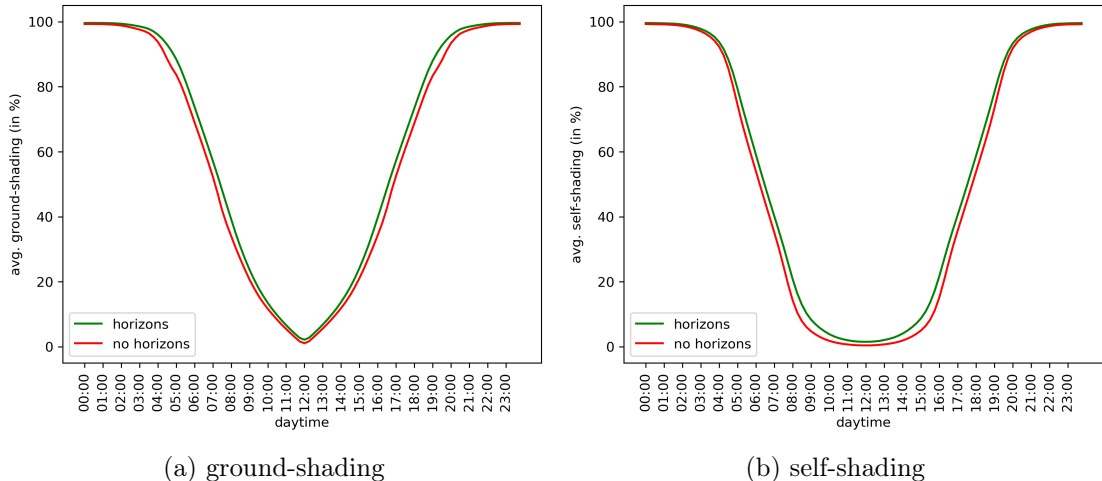


Figure 3.6.: Shading in vertical system by daytime with and without horizons

### 3. Results

Figures 3.6 show a comparison for the vertical system. Similar trends are present for all other systems, see A.3.

As expected, the shading is higher under the inclusion of horizons due to later sunrises and earlier sunsets and shading values being set to 100% during nighttime. Generally the difference in the two lines is very small. The data is averaged over the whole of Europe, where shading on most land areas is not strongly influenced by topography. However, it is important to keep in mind that differences in this figure would be significantly higher in mountainous regions.

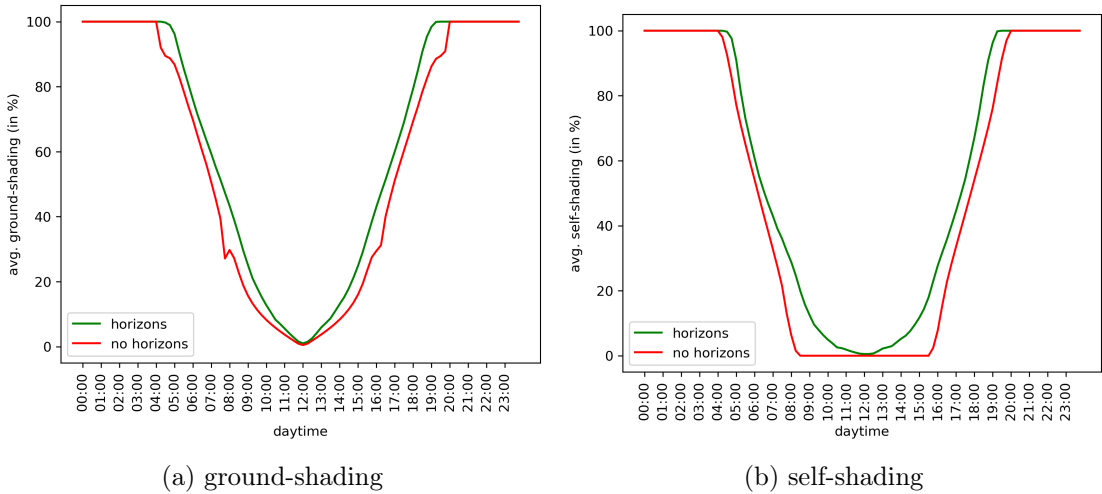


Figure 3.7.: Shading in vertical system by daytime with and without horizons for Ennstal region

Figure 3.7 shows the difference in ground- and self-shading under the inclusion/exclusion of horizon data for a valley in a mountainous region of Austria (Ennstal). The area under assessment is defined by a bounding box with corner point coordinates spanning latitudes from  $47.40^{\circ}$  to  $47.43^{\circ}$  and longitudes from  $13.63^{\circ}$  to  $13.83^{\circ}$ . During midday, when the elevation of the sun is at a high point, differences between both curves largely vanish, similar to 3.6. At other times of the day shading is noticeably increased for this region. Irregularities in the curve excluding horizon data are - again - caused by the field boundaries and the way shade is projected during sunrise and sunset. Their disappearance in the data including horizons confirms that they are produced during times of low sun elevation.

#### 3.1.3. Average Shading Over One Year

Figures 3.8a and 3.8b show how ground- and self-shading change over the course of one year in the simulated PV setups. The results for self-shading in the tracking and vertical systems are largely similar, with overlapping curves in Figure 3.8b.

Ground-shading in all systems is lower during the summer months and higher during

### 3.1. Average Shading

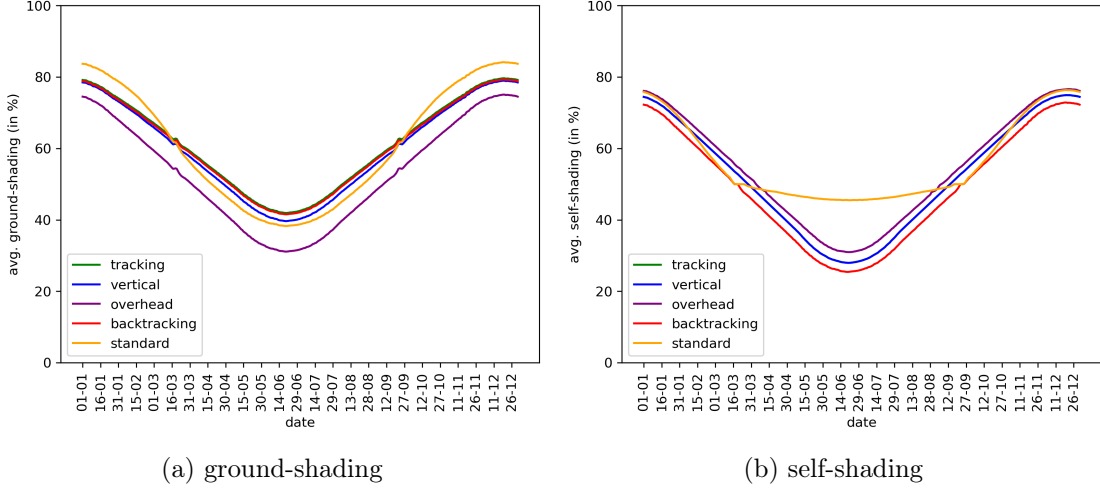


Figure 3.8.: Shading over one year

winter. The results are relatively similar across systems, with the exception of the overhead system, which, compared to the other systems, produces reduced ground-shading across the whole year. This fits with results described in previous sections. Another deviation from the general trend are the results from the standard system, which produces higher ground-shading than the tracking, backtracking and vertical systems in winter and lower ground-shading than these systems in summer (see 3.8a). The difference in comparison to the other systems is due to the different orientation of panel rows, with those in the standard system being aligned with the east/west direction, while those in the other systems are north/south aligned. In winter, ground-shading in the standard system is on average higher, due to lower variation in the azimuth, meaning the sun is consistently located closer to the south direction, with the reverse being true in summer. This was described in more detail in the previous section.

With respect to self-shading, there is a similar trend with lower self-shading occurring during summer. The backtracking system is always positioned to produce 0% self-shading, with the value being set to 100% at night. With almost all other systems following the same trend, it is clear that the overall trend is mostly caused by the change in daytime hours.

An interesting exception to this general trend occurs in the standard system. Average self-shading in this system is dramatically less impacted by day length during the summer months, specifically starting around the spring equinox (19. – 21. March) and ending around the fall equinox (22. – 24. September). This also matches closely with the beginning and end of polar day at the north pole. The differing trend in the standard system's self-shading is likely caused by this. The low elevation of the sun combined with its position in the south at high latitudes during all hours of the day would lead to a high amount of self-shading in the east/west aligned system, while systems aligned across the north/south direction remain unaffected.

### 3. Results

There is an overlap in self-shading in the tracking and vertical systems here, which is a result of the similar positioning of the tracking system close to sunrise and sunset, when most self-shading occurs.

One last notable abnormality, which is visible in Figure 3.8a, is the slight increase in shading around mid March and September before continuing along the general trend. This is presumably due to the occurrence of the aforementioned spring and fall equinox and the limitations presented by the predefined field borders. Around the equinox, the position of the sun is causing a higher amount of the shade projected by photovoltaic panels to fall within the set field area. Southern latitudes likely are more affected by this effect, due to higher sun elevation.

Figures 3.9a and 3.9b show differences between the average yearly course of ground- and self-shading when horizon data included and when it is excluded. For these figures, data which does not factor in horizons has been weighted to match the distribution latitudes present in the mastergrid.

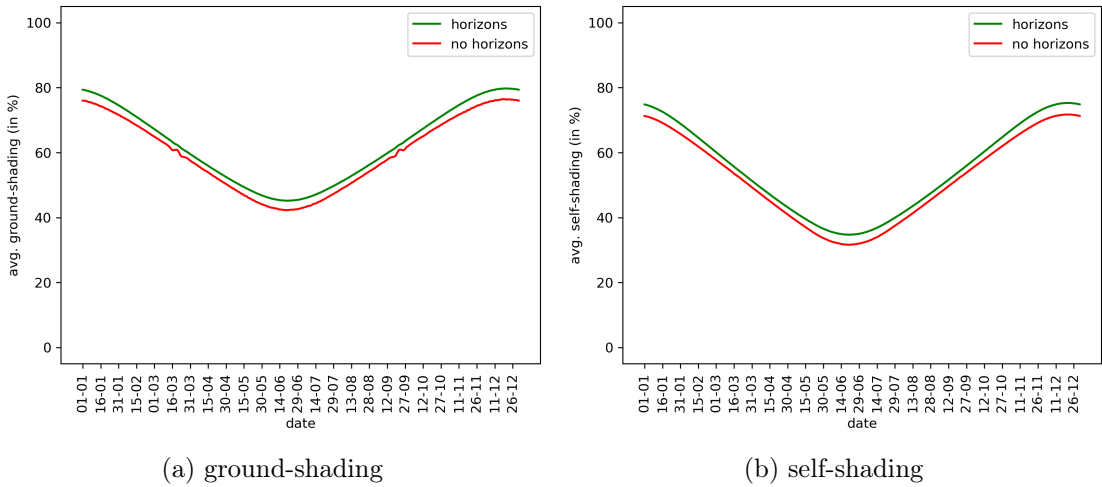


Figure 3.9.: Shading in vertical system by date with and without horizons

Figures 3.9 show a comparison for the vertical system. Similar trends are present for all other systems, see A.4. As in the previous case (3.6), the inclusion of horizon data produced slightly elevated levels of shading, which is to be expected. Another noticeable difference between the two curves is the disappearance of the irregularity around the time of the equinox in the one factoring in horizon data. This points to the irregularity being caused during times of low sun elevation and supports previous assumptions.

## 3.2. Illuminated Time

In Figure 3.10 the illuminated time for all mastergrid cells at different times of the year, as determined by horizon data and sun position, is depicted.

### 3.2. Illuminated Time

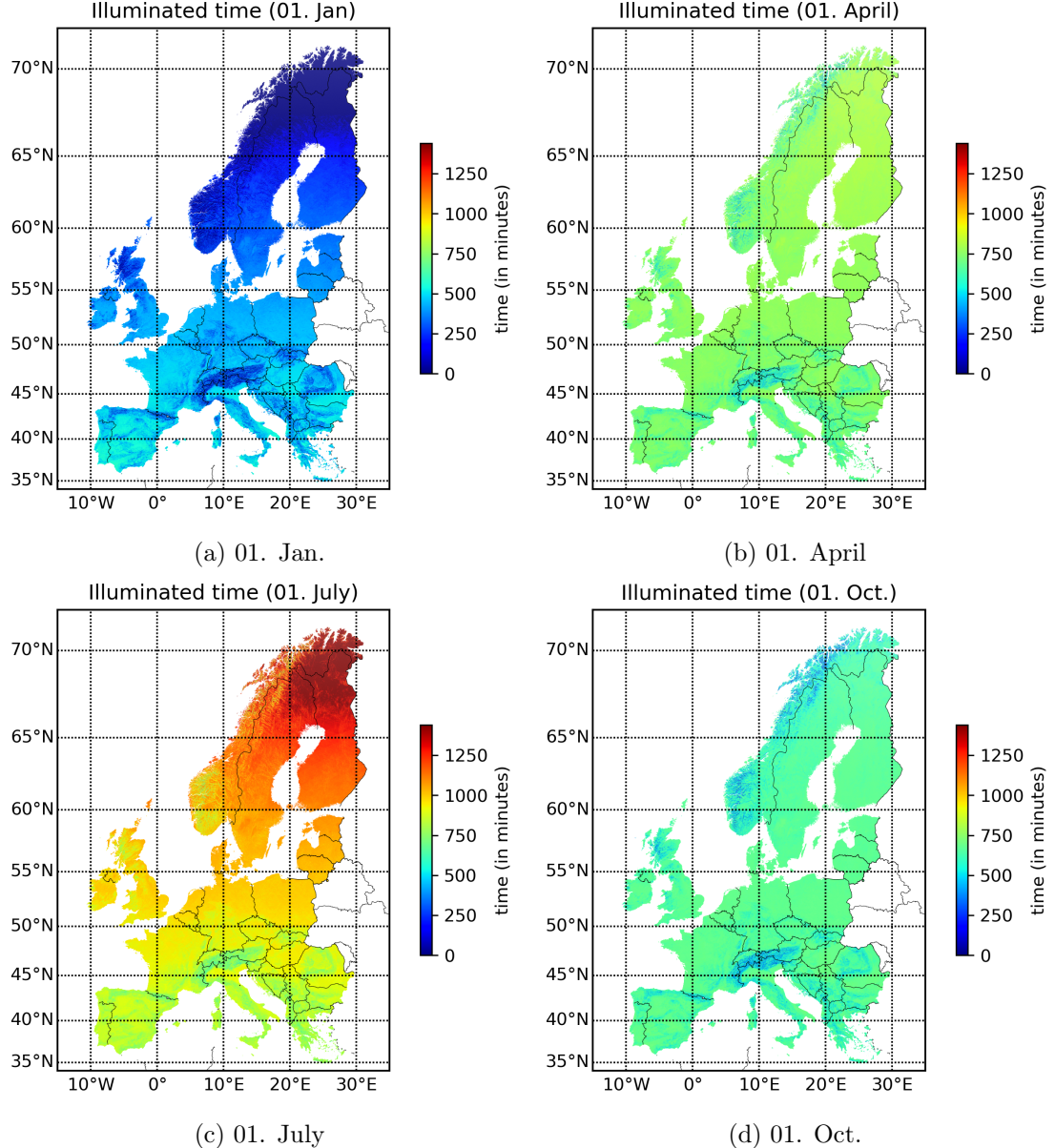


Figure 3.10.: Illuminated time across Europe

The calculated maps regarding total illuminated time confirm expectations, namely overall increased day lengths in summer. The polar circle is also visible in the figures for January and July. The generated maps clearly reflect the topography, with decreased day-lengths in hilly terrain, as expected.

The most dynamic stability in illuminated time can be found in Southern Europe, particularly Spain and Portugal, values here range between approximately 8.5 hours of

### 3. Results

daytime in winter to 14 hours in summer. Differences between seasons increase with rising latitude, with the extremes being polar day and night.

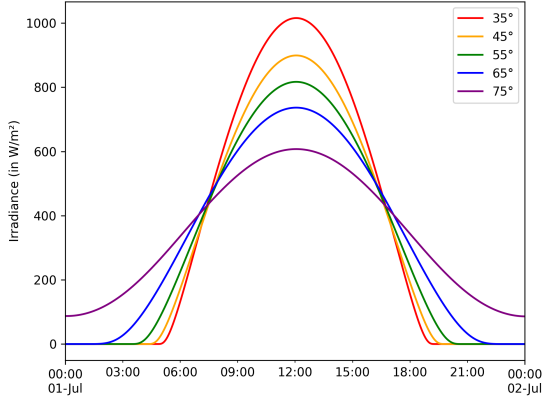


Figure 3.11.: Global horizontal irradiance under clear sky conditions on the 1<sup>st</sup> of July at different latitudes

While daytime hours are increased during summer months in northern regions, it is important to note that peaks in solar irradiance decrease with latitude, due to the relative position of the sun. A depiction of the influence of latitude on solar irradiance can be seen in Figure 3.11. Additionally, systems with north/south aligned panel rows would yield increasingly suboptimal results at higher latitudes. This is because of the consistently low elevation of the sun causing the angle between incoming sunbeams and photovoltaic panels to be far from normal. As discussed in the previous section, self-shading in the standard system may also be relatively high at increasingly northern latitudes. To mitigate this, panels would need to be spaced further apart. Regardless of the chosen system, electricity generation during winter months would be increasingly negatively affected at higher latitudes.

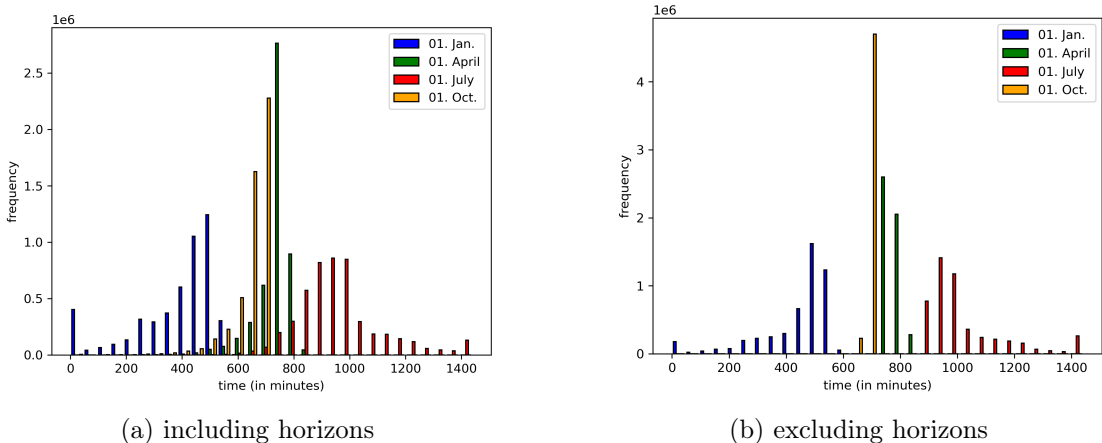


Figure 3.12.: Distribution of illuminated time across Europe

### 3.3. Distribution of Field Shading

3.12a shows the distribution of illuminated time for the cells of the used grid.

The distribution of illuminated time for different months is shown in Figure 3.12a. As to be expected, the distribution is similar for April and October, with little overlap between January and July. One notable aspect of this figure is the amount of locations experiencing 24 hours of daylight in July when compared to those receiving no sunlight in January. The significantly lower number of the former can be explained by the influence of horizons, especially in combination with low solar elevation.

As expected, Figure 3.12b, which excludes the influence of horizons, reveals a much more symmetrical distribution of illuminated time between January 1st and July 1st. It also displays a significantly narrower spread of illuminated time for April and October, highlighting the substantial impact that topographic horizons have on illumination variability.

## 3.3. Distribution of Field Shading

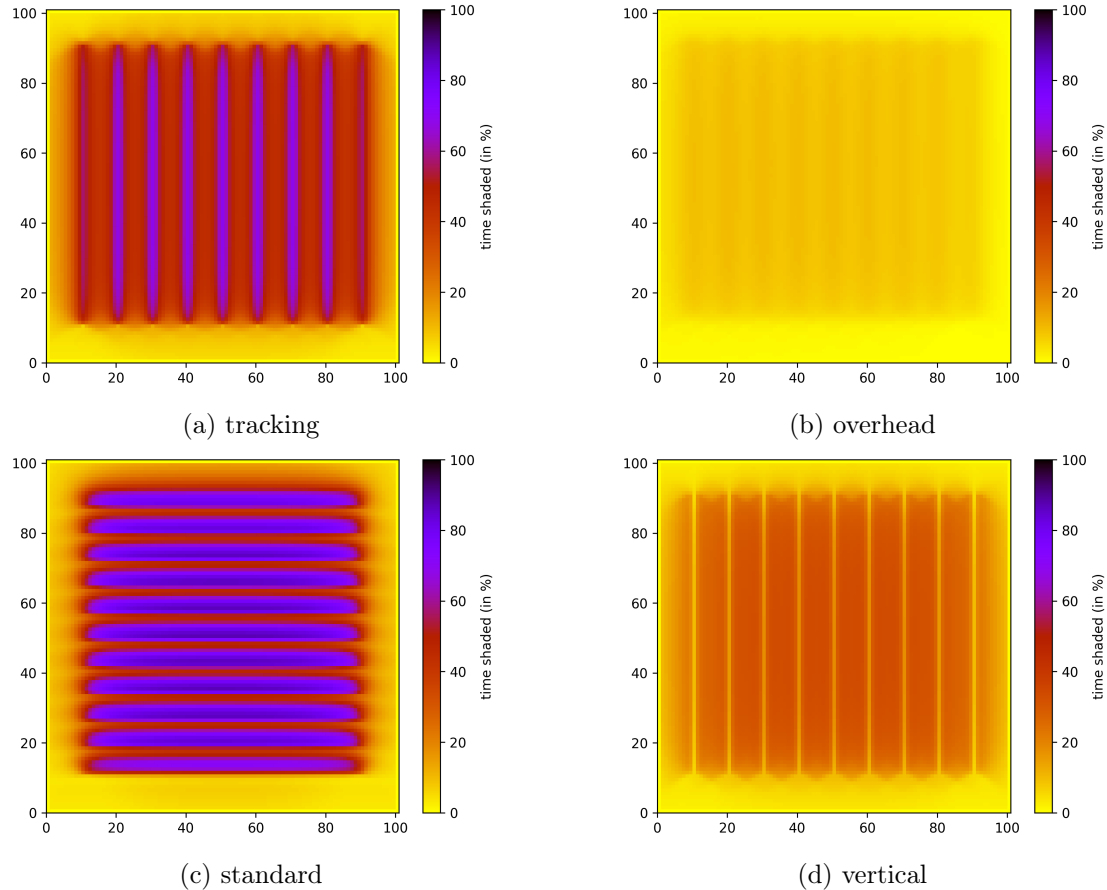


Figure 3.13.: Field shading in different systems

### 3. Results

The figures in 3.13 show how the simulated field is shaded assuming different system configurations. These results are averaged over one year. The percentages are determined in relation to daytime hours. Data shown in Figure 3.13 is averaged over all of Europe, horizon data was not considered for these results.

The distribution of field shading in the simulated systems is shown in Figure 3.13. The distribution in the tracking and backtracking system (see A.5) is largely similar, which is to be expected, since positioning in the two setups only differs if self-shading occurs in the tracking system. This is only the case for a short amount of time close to sunrise and sunset.

Overall the lowest shading can be seen in the overhead system, which coincides with results presented in previous sections. The areas affected most by shading in this system are those near the panel rows, but shading is distributed relatively evenly.

The highest overall shading can be found in the standard system, this is in accordance with previous findings as well. As mentioned before, panel positioning in this system is optimised for power generation and consequently leads to high ground-shading. To reduce this effect, panels could be placed further apart. However, peaks in ground-shading near the panel rows would likely remain, calling the viability of use alongside cropland into question. Use in combination with animal husbandry may be a better option. Another method of making this system more viable in the context of agrivoltaics may be to install panels in an overhead position - similar to the overhead system - to decrease shading.

In the tracking and backtracking systems, shade is also concentrated near where panel rows are placed. In between them, there is relatively even ground-shading, with the area being shaded around 40% of the time. Ground shading in this system can be reduced to similar levels as seen in the vertical system if similar parameters are used, see 3.14.

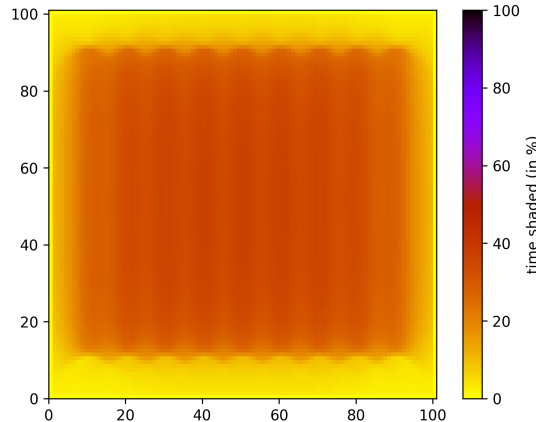


Figure 3.14.: Field shading in tracking system with altered parameters

The vertical system also shows relatively even shading, with the second lowest ground-shading values of the simulated systems. One noticeable abnormality in this system are the gaps in field shading where panel rows would be located. This is because, depending on the position of the sun, the shade occurring due to the panel is either projected to

### 3.3. Distribution of Field Shading

the east or the west of the panel. The only time shade would be projected at the same east/west position the panel is standing at by the panel itself, would be when the sun is positioned directly south. Additionally, field shading is not calculated continuously, instead discrete points are used. This leads to a rasterized effect in the Figures 3.13 and visually exaggerates the described effect.

The figures in 3.15 show how field shading develops by latitude. The categories on the right side of the plot give the amount of time an area is shaded over one year. The percentages on the x-axis describe the percentage of the total field area falling into the aforementioned categories. It is important to note, that an increased amount of categories was used for the overhead and vertical systems to make distinctions more visible in systems where ground-shading was generally lower.

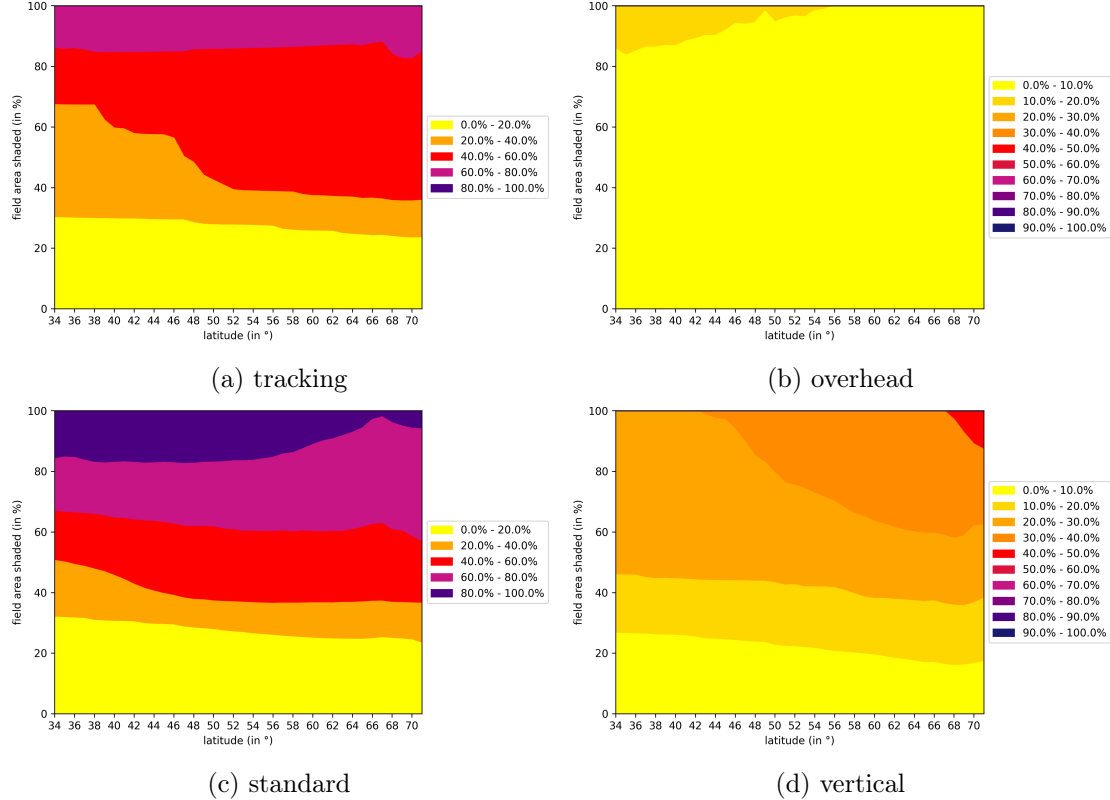


Figure 3.15.: Field shading changes by latitude

Results for the backtracking system largely resemble those for the tracking system (3.15a), the plot for the first can be found in A.5.

Figures showing the development of field shading by latitude (3.15) follow some general trends. There seems to be a slight increase in shading intensity at higher latitudes, which is corroborated by findings in 3.1.1, with the exception of the overhead system. With increasing latitude, the amount of area shaded 10 – 20% of the time decreases, with the

### *3. Results*

0 – 10% category taking over for this system. This is presumably due to decreased solar elevation leading to a higher portion of shade being projected outside the chosen field area. The effect is increased due to the large clearance in this system.

Generally, slight inconsistencies in development by latitude are likely because of the effects described in Section 3.1.1, being related to chosen time-steps and field borders. Irregularities around the polar circle can also be noted here. One notable development here is seen in the tracking system. Regarding the categories 20 – 40% and 40 – 60% of time shaded, there seems to be a relatively consistent development in shade distribution before a sharp increase at approximately 38°N and 46°N. A similar, but dampened trend can be seen in the backtracking system. This implies it likely occurs due to the behaviour of tracking systems, potentially especially because of behaviour close to sunrise and sunset, where the two systems differ.

## 4. Discussion

Generally, the results presented in the previous section match expectations, in particular with regards to the development of self- and ground-shading over the course of a day/year. The standard system resulting in the highest ground-shading values is unsurprising, considering that such systems are not necessarily intended to facilitate use alongside crops. The shading distribution (see 3.13), as calculated in the field shading simulation, coincides with irradiance patterns generated by others [23]. Irradiance reduction seems to be lower than the reduction in illuminated time, but this can be explained by higher shading in the morning and evening, where solar irradiation is lower. Additionally, field shading appears to be slightly lower in the single-axis tracking system than in the vertical system in [23]. However, as described in 3.3, this is highly dependent on the chosen system parameters. An example more similar to what is found in [23] can be seen in Figure 3.14. In [42] tracking and vertical systems with the same system parameters are shown to produce similar results regarding crop quality and yield, which also implies comparable shading conditions, matching with results found in this thesis. Moreover, the validity of the compiled horizon data and calculations of illuminated time, as seen in 3.2, can be confirmed by comparison to topographical data.

Regarding overhead systems, there is an additional factor to be considered in relation to ground-shading and its distribution. Depending on the chosen panel type, shading in these systems can be further reduced, if transparent panels are used. Panels used in these setups can have a transparency of 40 – 50% [36].

Another important factor to be taken into account regarding the presented results, is that, while ground- and self-shading are particularly high during times close to sunrise and sunset, these are also the times at which solar irradiance is relatively low (see Figure 3.11). As such, the impact of, for example, self-shading on electricity generation during these times, is much lower, than if the same shading were to occur during midday. The model used for shading calculations here could be further expanded through the inclusion of data on solar irradiance.

There are some limitations in the current model used for shading simulations. All simulations are done with the photovoltaic system assumed to be located on flat ground. In the future, inclined ground areas are an additional factor, which could be included in simulations, to extend the applicability of the simulation. To minimize computational effort, it may be possible to calculate the effect of inclined terrain generally, based on the slope and its direction, and use this to modify results based on topographical data. For example, a positive incline in the north direction may generally lead to higher ground shading, since, due to a relatively increased elevation of the sun, a higher proportion of

#### *4. Discussion*

total shade would be projected inside field boundaries. Potentially slope and direction in an inclined terrain could be generalized as representing a relative increase or decrease in shading values. Currently this is, however, a raw idea and would need to be confirmed before implementation. If this simplification is possible and values are overlaid with existing data, this would be a similar approach to the one chosen for horizon data.

Additionally, in the current model, panel rows can only be located along the north/-south or east/west directions. The systems included are also limited to being tilted along a single-axis with regards to self-shading calculations. Potential expansions would be finding a way to unify and expand self-shading calculations, such that dual-tilt systems are included and adding simulations of systems, which are not aligned along cardinal directions.

Further, this model could be expanded by calculating the amount of electricity generated in a given system. Alternatively, the data simulated with the shading model could be used to update data on generated electricity calculated using other models. Including both shading data and electricity generation in further studies would yield much more comprehensive results on the location dependent viability of systems. Another potential future addition to this model would be the inclusion of diffuse irradiation, as currently only the direct component of irradiation is considered.

In future work or when analysing specific locations, system parameters should be changed according to concrete local conditions, as seen in the comparison of field shading in tracking system (see 3.13 and 3.14). This may be of particular importance in regard to the tracking system, since it maximizes electricity generation, achieving a higher and temporally more evenly distributed yield [23, 42] when compared to the vertical system and can achieve similar ground shading with altered parameters.

With regards to agrivoltaics, the data generated with this model can be used for simulating crop growth in these setups. For this purpose, it is necessary to merge generated datasets containing the development of ground-shading data over time with datasets on irradiation.

In this thesis ground- and self-shading is calculated directly via the position of the sun and simulated photovoltaic panels. An alternative approach uses ray tracing. The former was chosen for the model presented here, as ray tracing is computationally much more expensive [24].

In this thesis, shade modelling was studied in the context of agrivoltaics, but the methods can be applied to different applications. For example, shading under photovoltaic systems over parking lots could be simulated, with the goal of finding ways to maximize the reduction in irradiation, particularly during mid-day. More generally, the model can be applied to topics beyond studying shading impacts of photovoltaic systems, as long as shading is simulated for structures that have a geometry comparable to photovoltaic panels.

## 5. Summary

Our analysis of shading by different photovoltaic systems across Europe shows that ground-shading was lowest in the overhead system, followed by the vertical system. Higher ground-shading was found in the tracking and backtracking systems, which yielded relatively similar results. The standard system leads to the highest ground shading. Additionally, shade distribution on the simulated field was particularly uneven in the standard system. This confirms that such a setup is less suited for agrivoltaic applications than other simulated systems, which cause lower and more evenly distributed ground shading. In a larger sense, this may be an issue regarding systems with east/west aligned panel rows. Further simulations are necessary to confirm this hypothesis.

These conclusions have been reached from data generated for all of Europe. It can be assumed that the viability of these systems varies depending on the chosen location. One example of this is the comparatively large increase of self-shading in the standard system at higher latitudes. Horizon profiles also have an impact on shading parameters, which depends highly on the chosen location. While generally increasing shading, detailed impacts need to be analysed on a location specific basis.

It is important to consider that shading varies strongly by region and that crops, which may be used in agrivoltaic setups, have a diverse set of needs. Moving forward, a particular focus of the analysis should be the adaptation of system parameters to meet location and crop specific requirements.

As shading parameters are highly dependent on chosen system parameters, and have been shown to affect how systems compare to each other for the vertical and tracking system, future studies should include potential electricity generation in the assessments of a system's viability at a given location. Systems not considered here may also be taken into account, e.g. overhead systems with east/west aligned panel rows, could be a more viable option at higher latitudes. Furthermore, shading data should be used to model differences in crop growth and quality. Future simulations on crop related factors based on shading data can be combined with data on electricity generation in different setups to reach more comprehensive results.

This is the first study comparing shading of five standardized systems (described in 2.2) across Europe. There is therefore a lack of data which can be used to validate the presented results against other simulations or against observations. Future work should address this shortcoming.



# Bibliography

- [1] P. E. Campana, B. Stridh, S. Amaducci and M. Colauzzi. Optimisation of vertically mounted agrivoltaic systems. *Journal of Cleaner Production*, 325:s.p. 2021. DOI: <https://doi.org/10.1016/j.jclepro.2021.129091>.
- [2] G. F. Jones, M. Evans and F. R. Shapiro. Reconsidering beam and diffuse solar fractions for agrivoltaics. *Solar Energy*, 237:135–143, 2022. DOI: <https://doi.org/10.1016/j.solener.2022.03.014>.
- [3] D. Coumou, A. Robinson and S. Rahmstorf. Global increase in record-breaking monthly-mean temperatures. *Climatic Change*, 118:3–4, 2013. DOI: <https://doi.org/10.1007/s10584-012-0668-1>.
- [4] IPCC. *Summary for policymakers*. In *Climate Change 2023: Synthesis Report. Contribution of Working Groups I, II and III to the Sixth Assessment Report of the Intergovernmental Panel on Climate Change [Core Writing Team, H. Lee and J. Romero (eds.)]* IPCC, Geneva, Switzerland, 2023, pages 1–34. DOI: <https://doi.org/10.59327/IPCC/AR6-9789291691647.001>.
- [5] L. Dias, J. P. Gouveia, P. Lourenço and J. Seixas. Interplay between the potential of photovoltaic systems and agricultural land use. *Land Use Policy*, 81:725–735, 2019. DOI: <https://doi.org/10.1016/j.landusepol.2018.11.036>.
- [6] R. Froese and J. Schilling. The nexus of climate change, land use, and conflicts. *Current Climate Change Reports*, 5:24–35, 2019. DOI: <https://doi.org/10.1007/s40641-019-00122-1>.
- [7] C. Aydinalp and M. S. Cresser. The effects of global climate change on agriculture. *American-Eurasian Journal of Agricultural & Environmental Sciences*, 3(5):672–676, 2008.
- [8] E. Grigorieva, A. Livenets and E. Stelmakh. Adaptation of agriculture to climate change: a scoping review. *Climate*, 11:202, 2023. DOI: <https://doi.org/10.3390/cli11100202>.
- [9] C. Dupraz, H. Marrou, G. Talbot, L. Dufour, A. Nogier and Y. Ferard. Combining solar photovoltaic panels and food crops for optimising land use: towards new agrivoltaic schemes. *Renewable Energy*, 36:2725–2732, 2011. DOI: <https://doi.org/10.1016/j.renene.2011.03.005>.
- [10] B. Willockx, C. Lavaert and J. Cappelle. Geospatial assessment of elevated agrivoltaics on arable land in europe to highlight the implications on design, land use and economic level. *Energy Reports*, 8:8736–8751, 2022. DOI: <https://doi.org/10.1016/j.egyr.2022.06.076>.

## Bibliography

- [11] C. Toledo and A. Scognamiglio. Agrivoltaic systems design and assessment: a critical review, and a descriptive model towards a sustainable landscape vision (three-dimensional agrivoltaic patterns). *Sustainability*, 13(12):6871, 2021. DOI: <https://doi.org/10.3390/su13126871>.
- [12] K. Mehta, M. J. Shah and W. Zoerner. Agri-pv (agrivoltaics) in developing countries: advancing sustainable farming to address the water–energy–food nexus. *Energies*, 17(17):4440, 2024. DOI: <https://doi.org/10.3390/en17174440>.
- [13] M. Trommsdorff, S. Gruber, T. Keinath, M. Hopf, C. Hermann, F. Schönberger, C. Gudat, A. T. Boggio, M. Gajewski, P. Högy, S. Zikeli, A. Ehmann, A. Weselek, U. Bodmer, C. Rösch, D. Ketzer, N. Weinberger, S. Schindele and J. Vollprecht. *Agrivoltaics: Opportunities for Agriculture and the Energy Transition - A Guideline for Germany / February 2024*. Fraunhofer ISE, Heidenhofstraße, Freiburg, 2024.
- [14] M. Vorast. *Challenges for Agrivoltaics in the International Context*. Master's thesis, University of Graz, Graz, Austria, 2022.
- [15] K. Ballarin. Viel mehr als nur Strom vom Acker. <https://www.schwaebische.de/regional/baden-wuerttemberg/viel-mehr-als-nur-strom-vom-acker-1571021>, 2023. Accessed: 2024-02-26.
- [16] A. Weselek, A. Bauerle, J. Hartung, S. Zikeli, I. Lewandowski and P. Högy. Agrivoltaic system impacts on microclimate and yield of different crops within an organic crop rotation in a temperate climate. *Agronomy for Sustainable Development*, 41:59, 2021. DOI: <https://doi.org/10.1007/s13593-021-00714-y>.
- [17] J. Vernier. *A coupling method using CFD, radiative models and a surface model to simulate the micro-climate - How to compute the impact of solar panels on the micro-climate within an agrivoltaic system*. Master's thesis, KTH Royal Institute of Technology, Stockholm, Sweden, 2023.
- [18] Y. Elamri, B. Cheviron, A. Mange, C. Dejean, F. Liron and G. Belaud. Rain concentration and sheltering effect of solar panels on cultivated plots. *Hydrology and Earth System Sciences*, 22:1285—1298, 2018. DOI: <https://doi.org/10.5194/hess-22-1285-2018>.
- [19] J. Ko, J. Cho, J. Choi, C.-Y. Yoon, K.-N. An, J.-O. Ban and D.-K. Kim. Simulation of crop yields grown under agro-photovoltaic panels: a case study in chonnam province, south korea. *Energies*, 14:8463, 2021. DOI: <https://doi.org/10.3390/en14248463>.
- [20] H. Jo, S. Asekova, M. A. Bayat, L. Ali, J. T. Song, Y.-S. Ha, D.-H. Hong and J.-D. Lee. Comparison of yield and yield components of several crops grown under agro-photovoltaic system in korea. *Agriculture*, 12:619, 2022. DOI: <https://doi.org/10.3390/agriculture12050619>.
- [21] T. Sekiyama and A. Nagashima. Solar sharing for both food and clean energy production: performance of agrivoltaic systems for corn, a typical shade-intolerant crop. *Environments*, 6:65, 2019. DOI: <https://doi.org/10.3390/environments6060065>.

## Bibliography

- [22] S. Kim, Y. Kim, Y. On, J. So, C.-Y. Yoon and S. Kim. Hybrid performance modeling of an agrophotovoltaic system in south korea. *Energies*, 15:6512, 2022. DOI: <https://doi.org/10.3390/en15186512>.
- [23] K. A. Niazi and M. Victoria. Comparative analysis of photovoltaic configurations for agrivoltaic systems in europe. *Progress in Photovoltaics*, 31:1101–1113, 2023. DOI: <https://doi.org/10.1002/pip.3727>.
- [24] O. A. Katsikogiannis, H. Ziar and O. Isabella. Integration of bifacial photovoltaics in agrivoltaic systems: a synergistic design approach. *Applied Energy*, 309:118475, 2022. DOI: <https://doi.org/10.1016/j.apenergy.2021.118475>.
- [25] European Commission. Photovoltaic geographical information system. [https://jrc.ec.europa.eu/pvg\\_tools/en/](https://jrc.ec.europa.eu/pvg_tools/en/). Accessed: 2025-02-26.
- [26] K. Anderson, C. Hansen, W. Holmgren, A. Jensen, M. Mikofski and A. Driesse. Pvlib python: 2023 project update. *Journal of Open Source Software*, 8(92):5994, 2023. DOI: <https://doi.org/10.21105/joss.05994>.
- [27] I. Grabner. Agri-PV - Ground- and Self-Shading. [https://github.com/isagrabner/agri-pv\\_ground\\_and\\_self\\_shading](https://github.com/isagrabner/agri-pv_ground_and_self_shading), 2025. Accessed: 2025-05-14.
- [28] A. Sarr, Y. M. Soro, A. K. Tossa and L. Diop. Agrivoltaic, a synergistic co-location of agricultural and energy production in perpetual mutation: a comprehensive review. *Processes*, 11:948, 2023. DOI: <https://doi.org/10.3390/pr11030948>.
- [29] S. Amaducci, X. Yin and M. Colauzzi. Agrivoltaic systems to optimise land use for electric energy production. *Applied Energy*, 220:545—561, 2018. DOI: <https://doi.org/10.1016/j.apenergy.2018.03.081>.
- [30] A. Magarelli, A. Mazzeo and G. Ferrara. Fruit crop species with agrivoltaic systems: a critical review. *Agronomy*, 14:722, 2024. DOI: <https://doi.org/10.3390/agronomy14040722>.
- [31] J. H. Koekemoer, J. R. Bredell, G. Venter and J. Reinecke. Field measurements of wind load effects in a photovoltaic single-axis tracker mounting rail. *Journal of Wind Engineering & Industrial Aerodynamics*, 253:105876, 2024. DOI: <https://doi.org/10.1016/j.jweia.2024.105876>.
- [32] SecondSol. Bescheinigung - Canadian Solar - CS3W-420P HiKu. <https://www.secondsol.com/de/anzeige/27884//canadian-solar/cs3w-420p-hiku-420wp>. Accessed: 2024-12-13.
- [33] M. Bruno. *Tracking Optimization in Agrivoltaic Systems - A Comparative Study for Apple Orchards*. Master's thesis, KTH Royal Institute of Technology, Stockholm, Sweden, 2023.
- [34] C. Mikovits, T. Krexner, I. Kral, A. Bauer, T. Schauppenlehner, M. Schönhart, E. Schmid and J. Schmidt. The contribution of agricoltaics to reaching climate neutrality in austria: combined simulation of electricity and crop outputs of agrivoltaic systems (unpublished manuscript). 2024.

## Bibliography

- [35] C. Hanisch and A. Steinhueser. First agrivoltaic system for carbon-neutral orcharding being tested. <https://www.ise.fraunhofer.de/en/press-media/press-releases/2021/first-agrivoltaic-system-for-carbon-neutral-orcharding-being-tested.html>, 2021. Accessed: 2025-04-04.
- [36] H. Süß. Sonnendach für die Apfelplantage. <https://www.wochenblatt-dlv.de/feld-stall/energie/sonnendach-fuer-apfelplantage-569265>, 2022. Accessed: 2024-12-13.
- [37] Halogenkauf LIGHTECH. Bescheibung - plentiSOLAR - Excellent Glass/Glass 170 M35. <https://www.plentisolar.de/51-transparentes-glass-glass-pv-modul-170wp-solarpanel-rahmenlos-ueberkopfmontage/a-1051754>. Accessed: 2024-12-13.
- [38] M. Z. Jacobson and V. Jadhav. World estimates of pv optimal tilt angles and ratios of sunlight incident upon tilted and tracked pv panels relative to horizontal panels. *Solar Energy*, 169:55–66, 2018. DOI: <https://doi.org/10.1016/j.solener.2018.04.030>.
- [39] J. Macknick, H. Hartmann, G. Barron-Gafford, B. Beatty, R. Burton, C. S. Choi, M. Davis, R. Davis, J. Figueroa, A. Garrett, L. Hain, S. Herbert, J. Janski, A. Kinzer, A. Knapp, M. Lehan, J. Losey, J. Marley, J. MacDonald, J. McCall, L. Nebert, S. Ravi, J. Schmidt, B. Staie and L. Walston. The 5 Cs of Agrivoltaic Success Factors in the United States: Lessons From the InSPIRE Research Study. Golden, CO: National Renewable Energy Laboratory. <https://www.nrel.gov/docs/fy22osti/83566.pdf>, 2022. Accessed: 2025-04-04.
- [40] PV-24. Bescheibung - JA Solar - JAM54D40-450/LB. <https://www.pv-24.at/products/ja-solar-jam54d40-450-1b-bifacial-pv-modul/>. Accessed: 2024-12-13.
- [41] S. Gillies, C. van der Wel, J. van den Bossche, M. W. Taves, J. Arnott and B. C. Ward. Shapely: manipulation and analysis of geometric objects. <https://github.com/shapely/>. Accessed: 2025-04-07.
- [42] T. Reher, C. Lavaert, B. Willockx, Y. Huyghe, J. Bisschop, J. A. Martens, J. Diels, J. Cappelle and B. Van de Poel. Potential of sugar beet (*beta vulgaris*) and wheat (*triticum aestivum*) production in vertical bifacial, tracked, or elevated agrivoltaic systems in belgium. *Applied Energy*, 359:122679, 2024. DOI: <https://doi.org/10.1016/j.apenergy.2024.122679>.

# A. Appendix

## A.1. Panel Tilt in Standard System by Latitude

The panel tilts in table A.1 have been determined by using a linear fit on optimal tilt angles listed in [38] for relevant latitudes.

Latitude	$\beta_{N/S}$
34°	29.111°
35°	29.429°
36°	29.746°
37°	30.064°
38°	30.381°
39°	30.699°
40°	31.016°
41°	31.334°
42°	31.651°
43°	31.968°
44°	32.286°
45°	32.603°
46°	32.921°

Latitude	$\beta_{N/S}$
47°	33.238°
48°	33.556°
49°	33.873°
50°	34.191°
51°	34.508°
52°	34.826°
53°	35.143°
54°	35.461°
55°	35.778°
56°	36.095°
57°	36.413°
58°	36.730°
59°	37.048°

Latitude	$\beta_{N/S}$
60°	37.365°
61°	37.683°
62°	38.000°
63°	38.318°
64°	38.635°
65°	38.953°
66°	39.270°
67°	39.588°
68°	39.905°
69°	40.222°
70°	40.540°
71°	40.857°
72°	41.175°

Table A.1.: Panel tilt by latitude for standard system

## A. Appendix

### A.2. Average Shading Depending on Daytime - Monthly Comparison

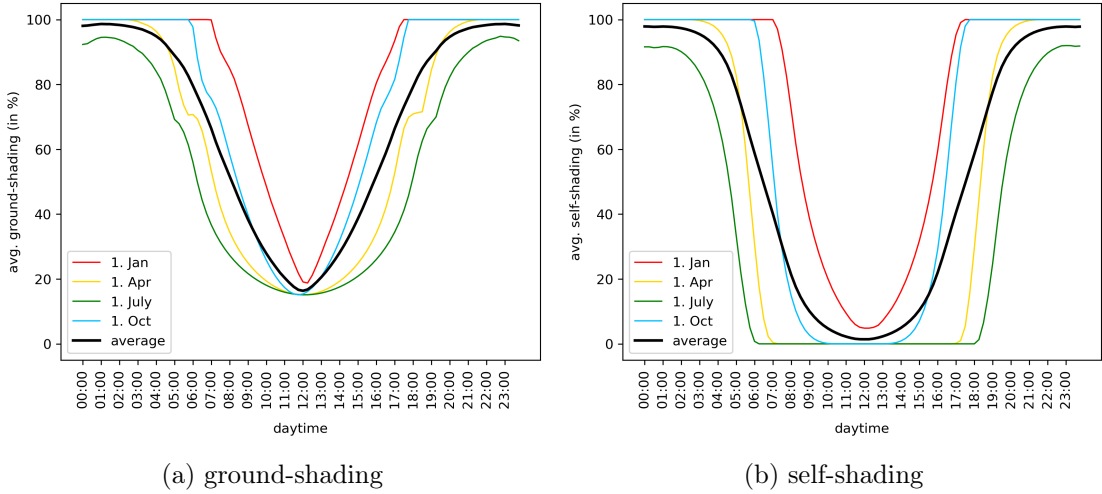


Figure A.1.: Shading by daytime at different times of the year in tracking system

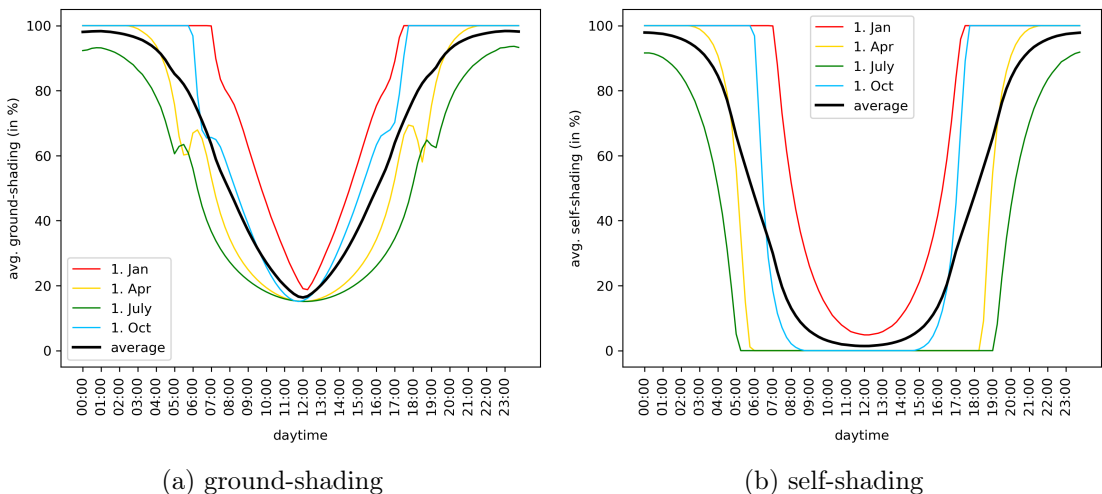


Figure A.2.: Shading by daytime at different times of the year in backtracking system

### A.2. Average Shading Depending on Daytime - Monthly Comparison

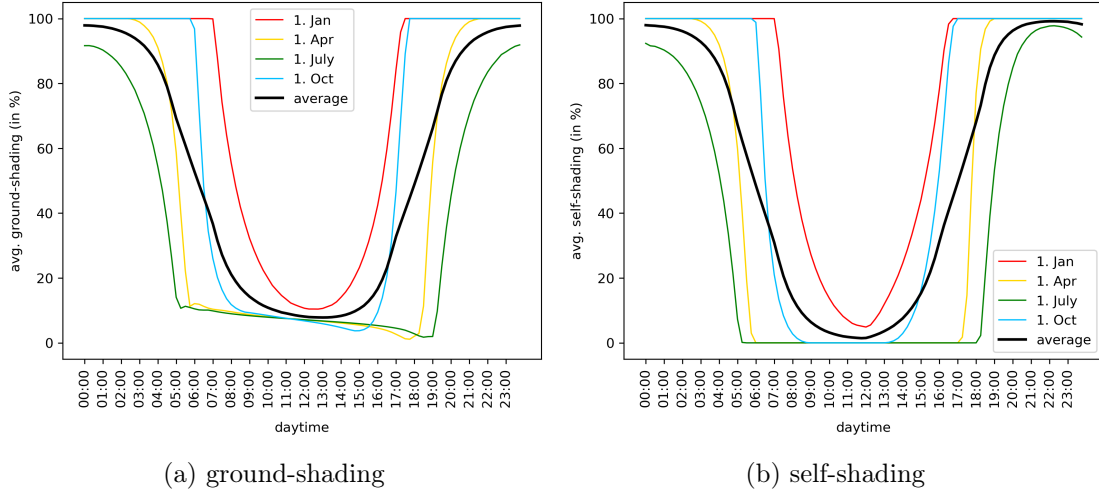


Figure A.3.: Shading by daytime at different times of the year in overhead system

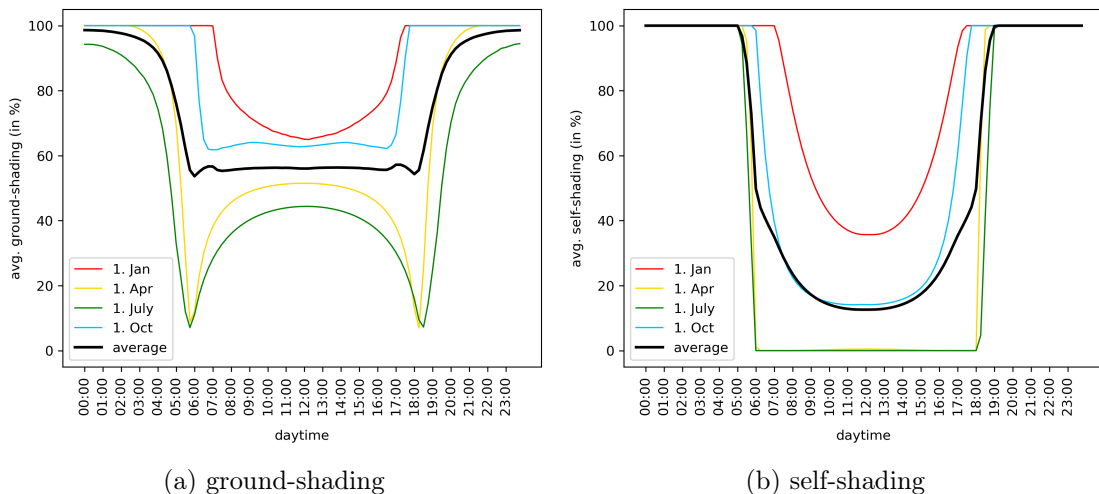


Figure A.4.: Shading by daytime at different times of the year in standard system

## A. Appendix

### A.3. Average Shading Depending on Daytime - Including/Excluding Horizons

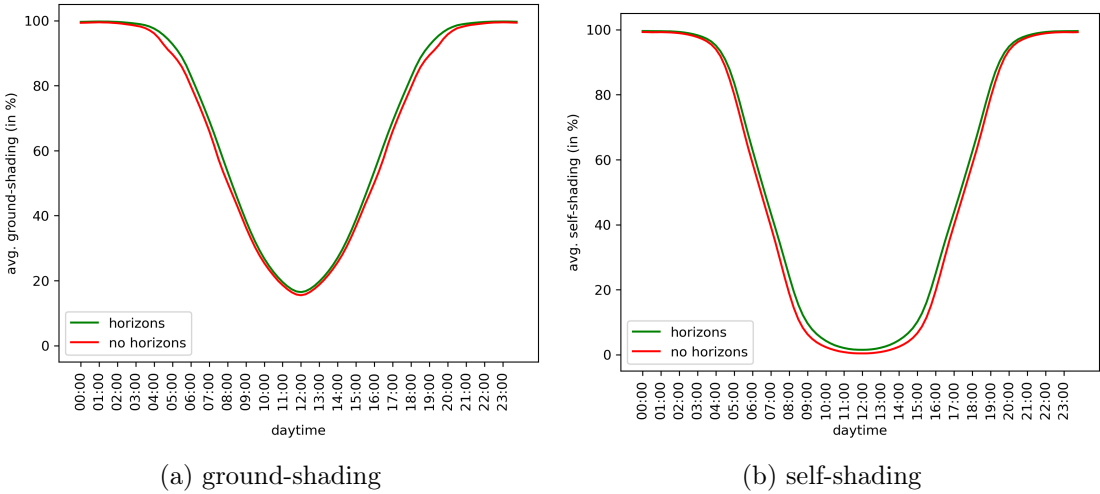


Figure A.5.: Shading in tracking system by daytime with and without horizons

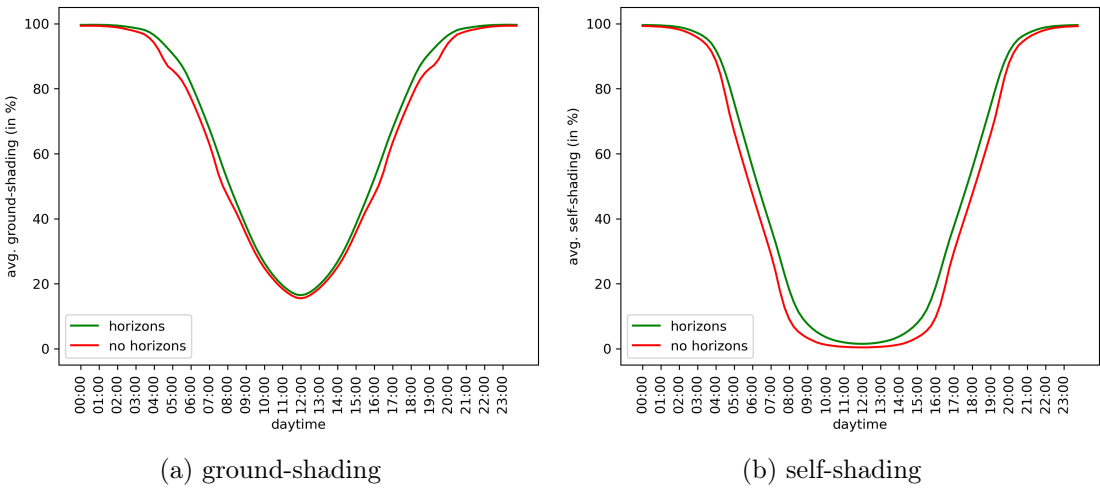


Figure A.6.: Shading in backtracking system by daytime with and without horizons

### A.3. Average Shading Depending on Daytime - Including/Excluding Horizons

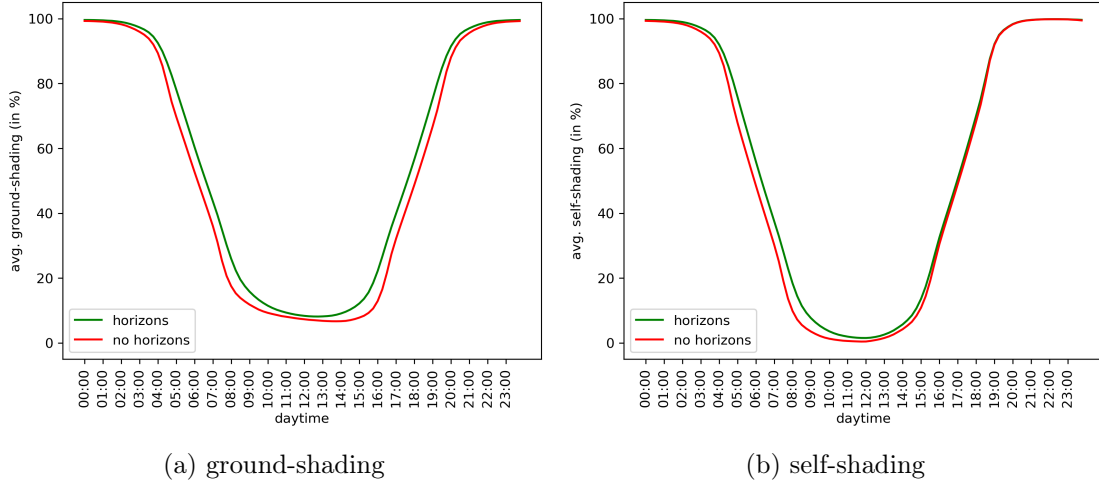


Figure A.7.: Shading in overhead system by daytime with and without horizons

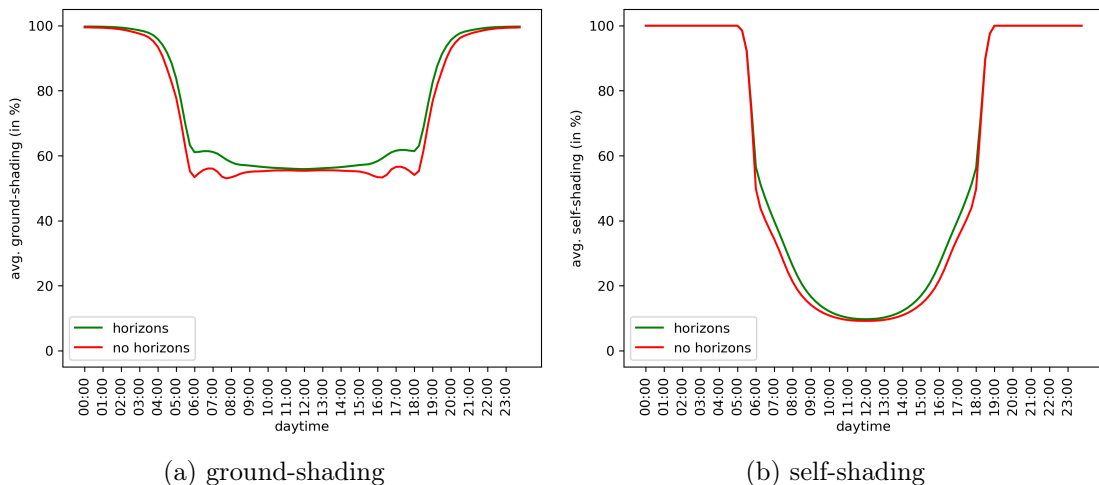


Figure A.8.: Shading in standard system by daytime with and without horizons

## A. Appendix

### A.4. Average Shading Depending on Date - Including/Excluding Horizons

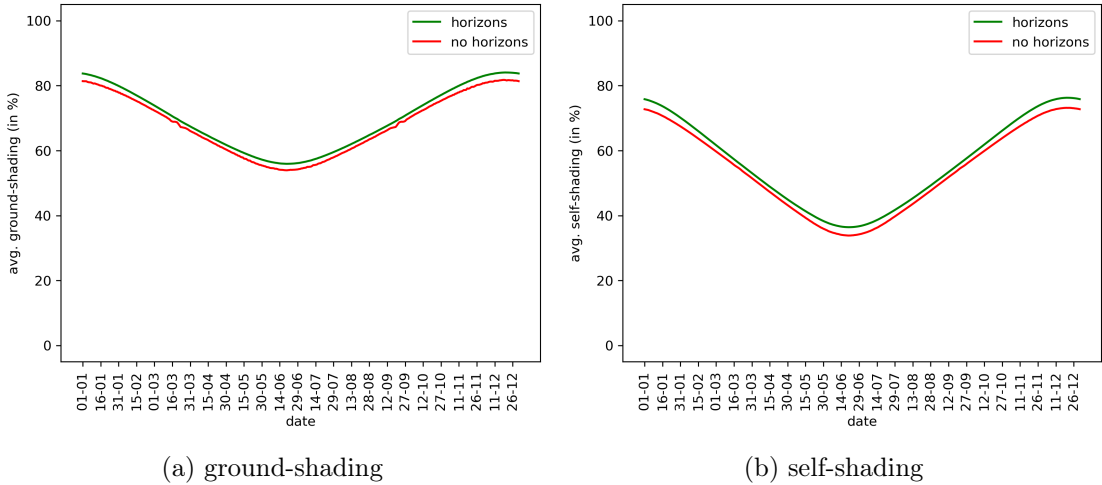


Figure A.9.: Shading in tracking system by date with and without horizons

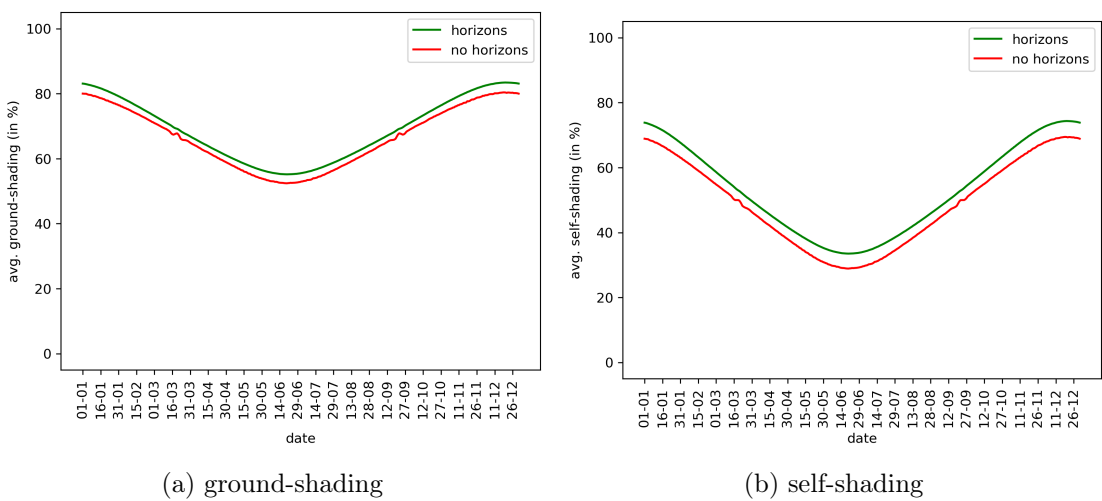


Figure A.10.: Shading in backtracking by date with and without horizons

#### A.4. Average Shading Depending on Date - Including/Excluding Horizons

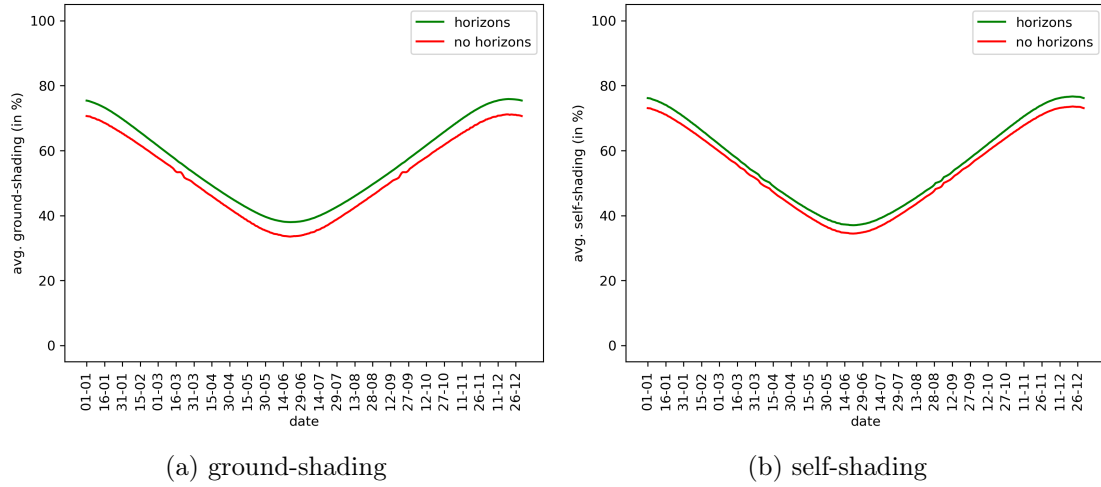


Figure A.11.: Shading in overhead by date with and without horizons

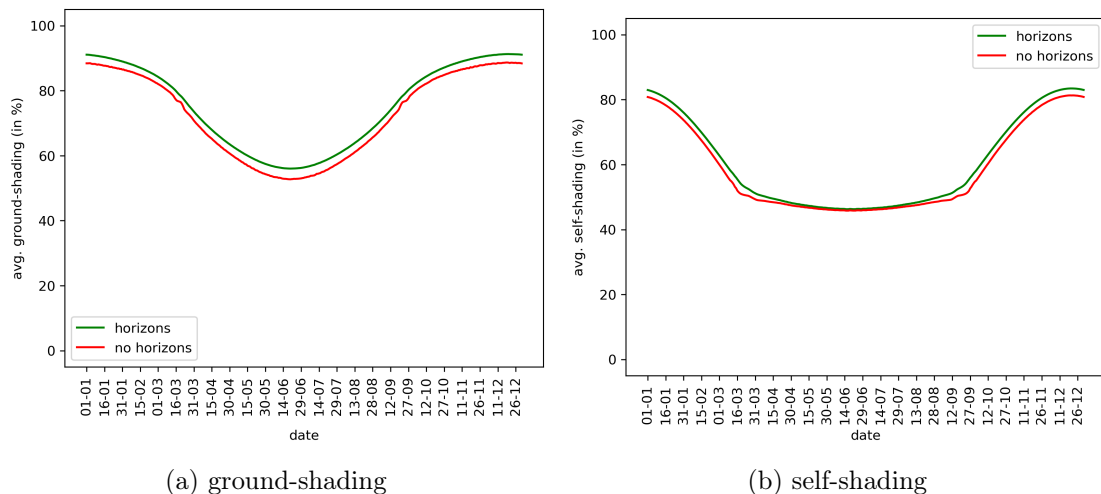


Figure A.12.: Shading in standard system by date with and without horizons

A. Appendix

### A.5. Field Shading - Backtracking

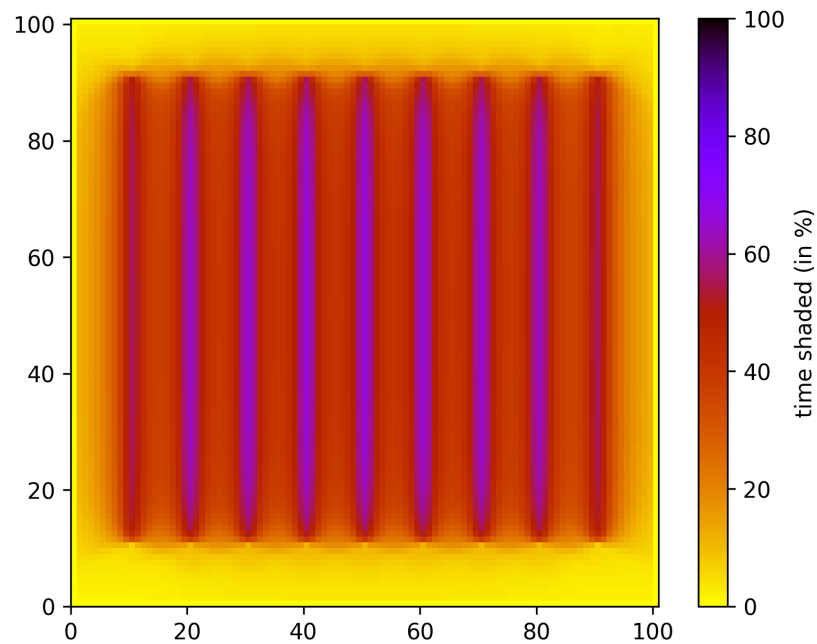


Figure A.13.: Field shading in backtracking system

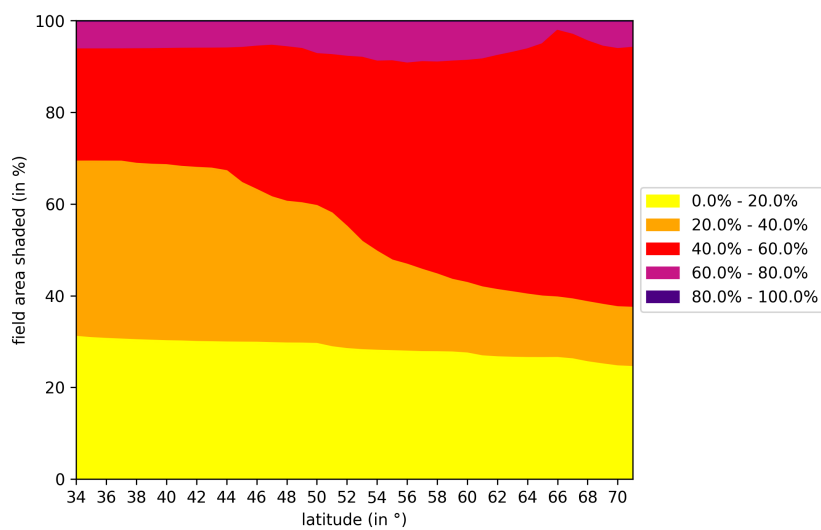


Figure A.14.: Field shading change by latitude in backtracking system